Marine and Petroleum Geology 63 (2015) 46–67

Contents lists available at ScienceDirect

Marine and Petroleum Geology

journal homepage: www.elsevier.com/locate/marpetgeo

Research paper

Depositional sequences, diagenesis and structural control of the Albian to Turonian carbonate platform systems in coastal Fars (SW Iran)

Benoit Vincent [a, *, 1], Frans S.P. van Buchem [b, 1], Luc G. Bulot [c], Mahmoud Jalali [d], Rudy Swennen [e], A.S. Hosseini [d], Darius Baghbani [d]

[a] Cambridge Carbonates Ltd, 1 rue de varoux, 21120 Marey-sur-Tille, France
[b] Maersk Oil Esplanaden 50, 1263 Copenhagen, Denmark
[c] Aix-Marseille University, UMR CNRS 7330 CEREGE, Centre St Charles, Case 67, 3 place Victor Hugo, 13331 Marseille Cedex 03, France
[d] NIOC R&D, No. 22, Negar Street, Vali-Asr Avenue, Vanak Square, Tehran, 19698-13771, Iran
[e] KUL Leuven, Celestijnenlaan 200 E B-3001 Heverlee, Belgium

ARTICLE INFO

Article history:
Received 19 September 2014
Received in revised form
11 February 2015
Accepted 13 February 2015
Available online 26 February 2015

Keywords:
Cenomanian
Turonian
Sarvak
Sequences
Carbonates
Diagenesis
Tectonics
SW Iran

ABSTRACT

This study covers a 300 km long, NE/SW oriented transect including five outcrop sections, and provides new biostratigraphic data and a sequence stratigraphic interpretation of the Albian, Cenomanian and Turonian sediments (Kazhdumi and Sarvak Formations) present in Coastal Fars (SW Iran). Two different carbonate depositional systems are distinguished, one for the Albian and one for the Cenomanian/Turonian. During the Albian eustatic control was the dominant factor influencing sedimentation, while during the Cenomanian and Turonian large and small scale tectonics were dominant. This resulted in significant thickness variations and local diagenetic overprint of the sequence boundaries.

Regional correlations were established constrained by ammonite data, as well as sedimentological and sequence stratigraphic considerations. In the Albian interval, including the Kazhdumi Formation and redated Mauddud Member, three 3rd order sequences have been distinguished. The depositional system consists of muddy carbonate ramps, rich in orbitolinid benthic foraminifers, which laterally interfinger with green marls. Albian deposits are present throughout the area and vary in thickness from 100 to 160 m. Subaerial exposure has only been observed on top of the Albian-3 sequence (Top Mauddud Member).

In the upper part of the succession, which is of Cenomanian/Turonian age, the depositional system changed to rudist-rimmed carbonate platforms surrounding local organic-rich, intra-shelf basins. The thickness in this interval varies greatly, from 0 to 300 m, which was controlled by both large scale (Qatar-Fars high) and local scale (salt domes) tectonic processes. In this tectonically active setting, three Cenomanian and one Turonian 3rd order sequences have been distinguished. Several sequence boundaries show evidences for long-lasted subaerial exposures (up to 13 Ma), with the local preservation of soil sequences and continental deposits. The expression of these exposures varies laterally considerably, and macroscopic evidences are sometimes lacking. Petrographic and C & O stable isotope investigations supplement classic sedimentology to reveal the record of these exposures.

1. Introduction

The mid Cretaceous Albian–Cenomanian–Turonian time interval is characterised on the Arabian plate by the presence of extensive shallow water carbonate deposits as well as the presence of organic-rich intrashelf basins which form the key components of some of the world's most prolific petroleum systems (*e.g.* Murris, 1980). Well-known reservoirs of this stratigraphic interval

* Corresponding author. Tel.: +33 645084016.
E-mail addresses: benoit@cambridgecarbonates.co.uk (B. Vincent), frans.vanbuchem@maerskoil.com (F.S.P. van Buchem), rudy.swennen@ees.kuleuven.be (R. Swennen).
[1] Previously at IFP Geology-Geochemistry Division, 1-4 ave de Bois préau, 92852 Rueil-Malmaison, France.

http://dx.doi.org/10.1016/j.marpetgeo.2015.02.018
0264-8172/

include the Natih Formation in Oman, the Mishrif Formation in the UAE, the Mauddud and Khatiyah Formations in Qatar, and the Sarvak Formation in Iran (*e.g.* Al-Sharhan and Narin, 1997; Sharland et al., 2001; Bordenave and Hegre, 2005).

Sequence stratigraphic studies of these rocks that were carried out in tectonically quiet areas, established a framework of 3rd order depositional sequences that can be confidently correlated at the scale of the eastern Arabian plate (*e.g.* van Buchem et al., 1996, 2002, 2010; Immenhauser et al., 1999; Raven et al., 2010; Razin et al., 2010; Sharp et al., 2010). This sequence stratigraphic framework, calibrated in time, was recently used by van Buchem et al. (2011) to propose a revised correlation between these lithostratigraphic units on the Eastern Arabian Plate. In addition, van Buchem et al. (2011) proposed a distinction between two different depositional systems: the Albian depositional system, characterized by the development of low-angle, orbitolinid-dominated, muddy ramp systems (Orbitolina Limestones in the Kazhdumi Formation in Iran, and Mauddud Formation in Oman and Kuwait), and the Cenomanian/Turonian system, characterized by rudist rimmed platforms surrounding organic-rich intrashelf basins (*e.g.* upper part of the Sarvak, Mishrif and Natih Formations). This paper provides further evidence for this depositional model.

The importance of tectonic activity during the Cenomanian/Turonian interval is well known (*e.g.* Ricou, 1971; Ala, 1974; Setudehnia, 1978; Stonely, 1981 Piryaei et al., 2010, 2011) and has locally significantly overprinted the expression of the 3rd order depositional sequences. Setudehnia (1978) already demonstrated the large differences in preservation of the Sarvak Formation in Western Iran, which varies from a maximum thickness in the order of 900 m in the Ahwaz area to total absence in the Coastal Fars area. A major tectonic control during the Cenomanian-Campanian was the obduction of the ocean crust which took place along the south-eastern and eastern margins of the Arabian plate, and led to (a) the re-activation of regional deep-seated normal fault systems that separated large-scale regionally uplifted and subsiding terrains within the plate, and (b) local salt tectonic uplift, notably above the Pre-Cambrian Hormuz salt basin.

This paper focuses on the Albian to Turonian succession, exposed in the coastal Fars area, where the influence of both local salt tectonics as well as regionally uplifted terrains (Qatar-Fars High) can be observed in a number of seismic scale outcrops. The purpose of this paper is threefold, firstly to refine the understanding of the timing and scale of the syn-sedimentary tectonic activity, secondly to evaluate its impact on the expression of the depositional sequences, and thirdly to document the diagenetic and sedimentological expression of the sequence boundaries in this setting.

2. Geological setting

The Zagros Mountain chain, which stretches along a SE–NW trend throughout SW Iran, is the result of a complex, multi-phased, geodynamic evolution that affected the eastern margin of the Arabian plate from the Late Cretaceous to the Neogene. This deformation phase started with the obduction of Neo-Tethys ocean floor sediments during the Late Cretaceous, and continued until the Neogene, resulting in final closure of the Neo-Tethys and foreland basin deformation in a compressional regime in the Late Miocene, when the Arabian and Central Iranian plates collided (*e.g.* Alavi, 1991; Wennberg et al., 2007). Several tectonic units are distinguished in the SE–NW oriented belt and the study area is located southwest of the suture zone near the front of the Zagros folding (Fig. 1), where the Zagros is subdivided in two large structural zones separated by the High Zagros Fault. Superposed on this pattern are additional N/S oriented main basement-rooted faults (the Kazerun and Hendijan Fault systems) that were active at various times throughout the geological history, and separate the Fars province from the faster subsiding Dezful Embayment and Lurestan areas in the North-West (Fig. 1). The presence of Pre-Cambrian salts of the Hormuz Formation, limited to the West by the Kazerun Fault system, strongly influenced the nature of tectonic deformation in Fars (Fig. 1).

The coastal Fars province is located in the northern extension of the axis of the Qatar-Fars arch, a deep-seated tectonic structure that dates back to the Pre-Cambrian and has influenced sedimentation ever since (*e.g.* van Buchem et al., 2011). The orientation of this structure is parallel to the Kazerun and Hendijan Fault systems (Fig. 1).

The study area is located in a relatively low accommodation zone, compared to the high accommodation areas in Khuzestan and Lurestan province. For instance, in large parts of coastal Fars the upper part of the Sarvak Formation (Cenomanian/Turonian) is absent, whereas rocks of this age can reach a thickness of up to 1200 m in Khuzestan area in the North (James and Wynd, 1965; Setudehnia, 1978). During the Cretaceous, the coastal Fars area consisted for most of the time of shallow water carbonate platforms (Fahliyan, Dariyan, Sarvak, Ilam Formations; Fig. 2) which experienced several episodes of subaerial exposures of regional extent. During the Albian, carbonate sedimentation was interrupted by a phase of intrashelf marl deposits (Kazhdumi Formation; *e.g.* James and Wynd, 1965).

3. Material and methods

Five outcrop sections were studied, from NNW to SSE: Kuh-e-Khormuj, Kuh-e-Khartang, Kuh-e-Namak, Kuh-e-Asaluyeh, and Kuh-e-Gach (Fig. 1; Table 1). The Khormuj and Khartang sections are located on the northwestern flank of the Qatar-Fars high, whereas Asaluyeh and Namak sections are located on the structure. The Gach section is located on the southeastern flank of the structure.

Sedimentological logs were measured at the decimeter scale, and sequence stratigraphic interpretations were made following the sequence definition of Vail et al. (1991). Biostratigraphic samples were taken at 1.5 m intervals. Microfossil determination was carried out by A. Hosseini, and where applicable the biozonation of Wynd (1965) was used.

The diagenetic investigations were made at the macroscopic scale in the field, and on thin-sections using classical optical microscope and cathodoluminescence equipment. Several sedimentological and diagenetic elements (pebbles, cements) were sampled with a dentist microdrill under a binocular for carbon and oxygen stable isotope analysis ($\delta^{13}C_{carb}$, $\delta^{18}O_{carb}$), in order to investigate the diagenesis associated with sequence boundaries. In addition, a total of 255 carbon isotope analyses of bulk matrix micrites were carried out in 4 sections for chemostratigraphic and diagenesis purpose (Table 2): Khormuj (116), Asaluyeh (88 samples), Gach (42 samples), and Namak (9). All samples were analyzed at the Institute of Geology and Mineralogy, University of Erlangen-Nürnberg, Germany. Powders were reacted with 100% phosphoric acid at 75 °C using a Kiel III online carbonate preparation line connected to a ThermoFinnigan 252 mass spectrometer. Isotopic values are reported in the standard δ-notation in per mil relative to V-PDB (Vienna Pee Dee Belemnite) by assigning a $\delta^{13}C$ value of +1.95‰ and a $\delta^{18}O$ value of −2.20‰ to NBS19. Reproducibility was checked by replicate analysis of laboratory standards and is better than ±0.02‰ (1σ) for carbon isotope and ±0.05‰ (1σ) for oxygen isotope.

4. Sedimentology and stratigraphy

4.1. Depositional environments

The sedimentary facies description is based on macroscopic and microscopic observations on the faunal content and lithology, and

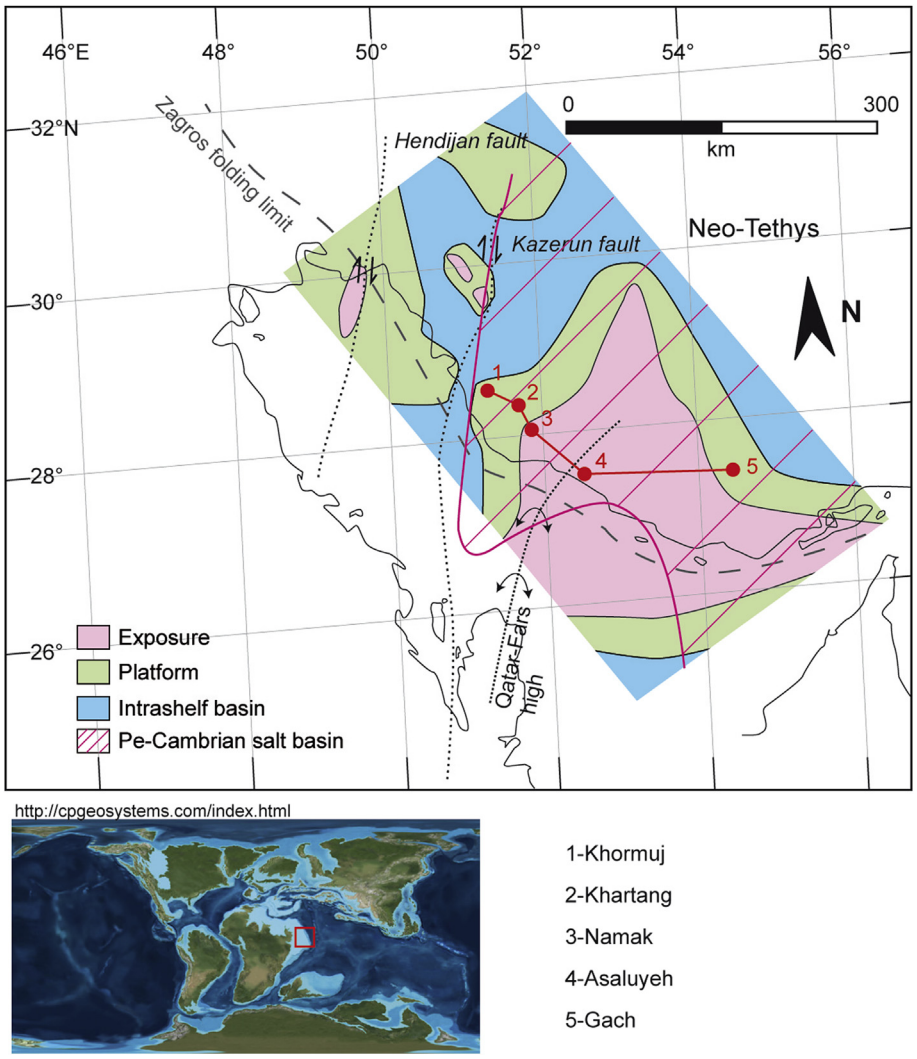

Figure 1. Location of the studied sections in the Zagros Mountains of southwest Iran shown on a paleogeographic map of the late Cenomanian (modified and simplified after non-published data). The location of the Qatar-Fars high is from Sharland et al. (2001).

field observations on sedimentological structures, depositional geometries and bedding patterns. The environmental interpretation relies on the microfossil content in combination with geometrical control (depositional profiles) provided by the seismic scale outcrops and the regional existing stratigraphic reconstructions. Two different depositional models each including several facies associations are distinguished, one for the Albian and one for the Cenomanian/Turonian. Noteworthy is that the present interpretations are coherent with already published paleoenvironment models for the Cenomanian-Turonian interval on the Arabian plate (*e.g.* van Buchem et al., 1996, 2002; Razin et al., 2010; Champagne, 2012; Mahdi et al., 2013).

4.1.1. Albian system – low angle, muddy carbonate ramps

4.1.1.1. Orbitolinid-rich wackestone to packstone (mid to inner ramp). These wackestone and packstone are organized in decimeter to meter scale beds, displaying a thin and slightly wavy bedding pattern (Figs. 3, 4, 5, 6). Fossil content can be abundant, in particular dominated by benthic foraminifers (orbitolinids, trocholinids), bivalve shells, and echinoderm fragments (Figs. 3, 4, 5).

4.1.1.2. Green marls (shallow intrashelf basin to outer ramp). The green marls locally display decimeter scale carbonate beds (Figs. 3, 4, 5, 6). Fossils are locally abundant, including small and large orbitolinids, bivalves (rarely in situ), echinoderms, and ammonites (Figs. 3, 4, 5).

4.1.2. Cenomanian/Turonian system – platform to intrashelf basin system

4.1.2.1. Pisoid-rich, quartz-rich red clays (continental). Paleosoil sequences were observed in Khormuj and Khartang sections, with internal pisoid and glaebule rich-layers and iron crusts. Locally erosive fluvial conglomerates and sandstones cut through the soil sequence (Figs. 3, 4).

4.1.2.2. Peloid-rich, bioclastic packstone to grainstone (low-energy platform top). In this facies association, bedding pattern varies from decimeter to meter scale (Fig. 6). Meter scale beds can be bioturbated, and fossil content includes small benthic foraminifers (mainly uni- and biseriated, and miliolids), gastropods, bivalve shells, and green algae (Figs. 4, 5). Micritisation of bioclasts is common. Rudist-dominated wackestone are locally also observed.

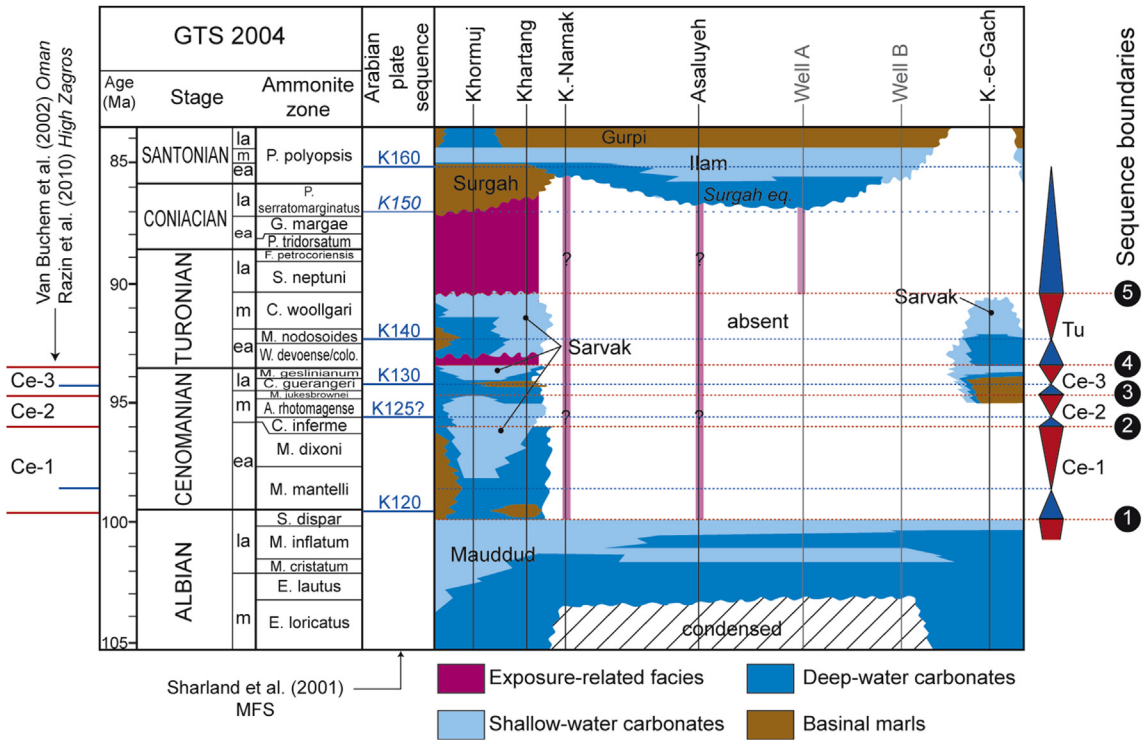

Figure 2. Revised Albian–Santonian lithostratigraphic scheme of the Fars province. Notable changes were made compared to James and Wynd (1965) based on age revision from collected ammonites (see the text for explanations).

This facies association illustrates a relatively low energy platform top environment.

4.1.2.3. Rudist grainstone to rudstone (high-energy platform margin). Two main kinds of bedding patterns characterize this facies association. Decimeter to meter scale beds, displaying cross-bedding with bed sets at the meter scale (Fig. 3), are interpreted as stacked sandwave units. Larger scale clinoforms with a depositional profile of 35–90 m (Fig. 7), correspond to prograding platform margin foresets. Bioclasts consist mostly of rudist debris, with additional echinoderm fragments, undetermined bioclasts, and small benthic foraminifers (Fig. 3).

4.1.2.4. Bioclastic mudstones and wackestone (toe of platform margin slope). The bedding pattern consists of thin, cm-scale, parallel beds with undulating bed tops (Figs. 3, 4, 6, 7). The lithology varies from marl to mudstone and wackestone with oysters, undetermined bivalves, rare echinoderm, orbitolinid fragments, as well as bryozoans. *Thalassinoides* burrows are common, and furrow and scour features indicate storm influence.

4.1.2.5. Grey marls (intrashelf basin). These uniform and mm-laminated marls and argillaceous mudstones contain ammonites, nautiloids, and planktonic foraminifers. Minimum water depth is estimated at around 80–90 m, based on laterally existing clinoform geometries (Fig. 7).

Table 1
Coordinates of outcrop sections studied in this work.

Sections	Latitude	Longitude
Khormuj	N28°39′21″	E51°24′14″
Khartang	N28°31′56″	E51°45′09″
Kuh-e-Namak	N28°15′16″	E51°46′38″
Kuh-e-Asaluyeh	N27°35′56″	E52°31′31″
Kuh-e-Gach	N27°34′46″	E54°30′06″

4.2. Sequence stratigraphic framework

The sequence stratigraphic framework was established taking into account biostratigraphic constraints (ammonites, benthic foraminifers), carbon isotope stratigraphy, the evolution of the depositional system, and the regional tectono-stratigraphic context. Interpretation of sequence stratigraphy, and used terminology, follow general principles (*e.g.* Mitchum and van Wagoner, 1991; Homewood et al. 1992; Strasser et al. 1999; Catuneanu, 2006). First the time constraints are presented, followed by the description of the depositional sequences.

4.2.1. Biostratigraphy and chemostratigraphy

A significant number of ammonites were encountered in the studied sections. The ammonites found in the Kazhdumi Marls and Orbitolina Limestones were already reported in Vincent et al. (2010a,b), and are summarized in Table 3. An abundant fauna found in the Sarvak Formation of the Khartang section is for the first time reported and described here (Fig. 3). Other more scattered assemblages were found in the other sections (Table 3). These findings are of fundamental stratigraphic significance for the dating of the lower part of the Sarvak Formation (the Mauddud Member). Stratigraphically significant species are illustrated in Figure 8.

In the Khartang section an ammonite fauna was collected from a 40 m thick succession of marls and nodular limestone alternations at the base of the Ahmadi Member which overlays the carbonates of the Mauddud Member (Figs. 4, 6). Most beds are fossiliferous but the fauna is more abundant at four different levels. The lower levels (KHA S01, KHA S02) lie about 15 m above the top Mauddud and contain exclusively *Utaturiceras* gr. *vicinale* (Stolizka). Ten meters above, another level (KHA S03) is characterized by abundant

Table 2
Stable isotope results.

Khormuj section						Asaluyeh section				Gach section	
Bulk curve				Xtra profile Figure 16							
$\delta^{13}C$ (‰ vPDB)	$\delta^{18}O$ (‰ vPDB)	$\delta^{13}C$ (‰ vPDB)	$\delta^{18}O$ (‰ vPDB)	$\delta^{13}C$ (‰ vPDB)	$\delta^{18}O$ (‰ vPDB)	$\delta^{13}C$ (‰ vPDB)	$\delta^{18}O$ (‰ vPDB)	$\delta^{13}C$ (‰ vPDB)	$\delta^{18}O$ (‰ vPDB)	$\delta^{13}C$ (‰ vPDB)	$\delta^{18}O$ (‰ vPDB)
1.67	−5.51	2.03	−3.84	2.48	−5.04	1.58	−3.47	3.10	−4.29	1.38	−6.39
1.94	−5.14	2.05	−3.88	2.86	−5.61	1.22	−3.72	3.18	−4.45	1.53	−6.21
1.85	−5.32	1.98	−4.23	2.32	−5.21	1.16	−3.87	2.89	−4.27	1.76	−5.85
1.79	−5.27	2.10	−3.60	2.27	−5.49	1.51	−3.54	3.11	−4.39	0.53	−5.08
1.74	−5.47	1.63	−4.37	1.96	−5.83	1.42	−3.56	2.77	−4.37	−0.56	−5.26
1.96	−5.29	2.14	−3.76	1.82	−6.17	1.45	−3.51	2.59	−4.43	−1.13	−8.42
1.86	−5.38	1.86	−3.88	2.25	−5.88	1.53	−3.53	2.91	−4.00	1.91	−6.00
1.64	−5.47	1.79	−4.40	−1.15	−5.34	0.52	−4.03	2.77	−4.11	1.98	−6.48
1.82	−5.38	1.82	−3.96	−4.37	−5.01	0.75	−3.69	2.33	−4.21	1.89	−5.60
1.21	−5.98	2.05	−3.66			0.88	−3.73	2.93	−4.69	1.72	−4.72
1.13	−5.98	1.69	−4.31	**Soil elements** (Fig. 15)		0.84	−3.97	2.82	−4.30	1.61	−3.63
0.63	−5.38	2.14	−3.99	**$\delta^{13}C$ (‰ vPDB)**	**$\delta^{18}O$ (‰ vPDB)**	0.17	−4.35	2.45	−4.36	1.44	−4.14
1.34	−5.46	1.53	−4.57	−7.76	−4.51	0.40	−4.13	2.35	−4.23	0.68	−4.77
1.50	−5.23	2.05	−3.82	−8.82	−4.87	0.76	−4.14	2.63	−4.34	0.64	−5.13
1.44	−5.31	2.34	−4.28	−7.41	−5.83	1.36	−4.44	3.12	−4.91	0.11	−3.46
1.75	−4.19	1.96	−3.92	−8.68	−5.12	1.39	−4.41	3.26	−4.00	−1.52	−4.27
1.67	−4.54	2.36	−3.48			1.37	−4.69	3.24	−3.91	0.33	−5.08
1.38	−5.00	2.22	−4.55			1.95	−5.33	3.19	−4.04	1.10	−4.00
1.59	−4.91	2.06	−4.62			1.52	−4.56	3.16	−4.72	0.72	−3.77
1.54	−5.19	2.10	−4.27			0.88	−4.60	3.18	−4.46	0.33	−4.31
1.59	−5.59	2.67	−3.79			1.30	−4.59	3.33	−4.08	0.58	−4.35
1.58	−5.50	1.88	−4.81			1.10	−4.42	3.01	−4.09	0.12	−4.39
1.24	−5.63	2.72	−4.32			2.05	−3.88	3.09	−4.01	0.35	−5.74
1.14	−5.68	2.59	−4.52			1.51	−3.84	2.97	−4.63	0.42	−4.88
0.66	−5.27	2.52	−4.46			1.78	−3.64	2.82	−4.22	0.86	−4.58
0.51	−4.91	2.27	−4.62			1.60	−4.11	2.61	−4.08	0.58	−3.84
0.75	−5.26	2.41	−4.36			3.05	−4.51	2.83	−4.55	0.63	−4.91
−1.07	−5.39	2.22	−4.64			1.08	−3.97	2.64	−4.35	0.75	−5.07
0.92	−4.14	1.87	−4.70			1.02	−4.02	2.69	−4.19	0.86	−4.84
0.49	−5.03	1.60	−4.77			1.78	−4.24	2.33	−4.37	1.33	−4.92
1.12	−5.32	1.45	−4.69			2.96	−3.44	2.70	−3.69	1.61	−2.17
0.98	−5.54	1.29	−4.08			2.05	−3.43	2.52	−3.90	2.10	−3.21
1.12	−5.07	1.15	−4.55			1.54	−4.18	2.38	−3.88	2.14	−3.29
1.06	−5.80	1.53	−3.36			2.12	−4.64			2.58	−4.00
1.11	−5.38	1.20	−3.82			1.82	−3.78			2.72	−4.16
0.90	−5.16	−2.89	−4.61			2.18	−4.66			2.35	−4.15
1.20	−5.55	0.67	−4.58			2.14	−4.19			3.26	−4.34
1.17	−5.06	1.33	−2.85			3.56	−4.30			3.09	−5.20
1.21	−5.20	1.36	−3.85			1.89	−4.52			2.75	−6.07
0.85	−4.08	2.19	−3.81			2.64	−4.31			3.43	−5.27
1.24	−5.06	1.77	−4.41			3.44	−4.31			1.30	−3.28
1.17	−5.73	2.24	−4.44			3.40	−4.18			1.07	−3.20
0.93	−5.46	2.96	−4.15			3.60	−4.18				
0.95	−5.42	3.94	−4.20			3.11	−4.41				
1.03	−5.18	3.04	−4.52			2.89	−4.67			**Namak section**	
1.70	−3.61	2.68	−4.00			3.05	−4.30			**$\delta^{13}C$ (‰ vPDB)**	**$\delta^{18}O$ (‰ vPDB)**
1.65	−3.94	2.59	−3.96			3.05	−4.04			2.33	−3.46
1.29	−3.57	2.49	−4.29			3.00	−4.30			2.53	−3.85
1.25	−4.45	1.38	−4.82			3.02	−4.12			2.05	−4.2
1.35	−4.33	0.33	−4.74			2.59	−4.13			2.22	−4.11
2.42	−3.99	1.13	−4.51			2.65	−3.97			2.46	−4.22
2.10	−4.14	−1.36	−4.41			2.67	−4.33			2.81	−4.15
1.70	−4.62					2.17	−3.82			2.9	−4.13
2.24	−3.69					2.67	−3.88			2.98	−4.52
2.25	−3.94					3.00	−4.09			3.21	−3.92

Utaturiceras gr. *vicinale* and *Sharpeiceras schlueteri* Hyatt. The fourth level (KHA S04) occurs about 10 m below the Sarvak limestone cliff (Figs. 4, 6) and is dominated by *Sharpeiceras*. This fauna indicates the Early Cenomanian *Mantelli* Zone. *Utaturiceras* has been reported to occur in the lower part of the Cenomanian in South India, Madagascar, the Middle East, southern England, Germany and Japan (see Matsumoto et al., 2003 for discussion). When well dated (Lewy and Raab, 1978; Wiedmann and Schneider, 1979; Wiedmann et al., 1989; Wright and Kennedy, 1996; Matsumoto et al., 2003), the genus is characteristic of the lowermost part of the Early Cenomanian (*Carcitanense* Subzone). *Sharpeiceras schlueteri* Hyatt first appears in the upper part of the *Carcitanense* Subzone and ranges to the upper part of the *Dixoni* Zone (Wright and Kennedy, 1987). The overlap between *Utaturiceras* and *Sharpeiceras* suggests that KHA S03 represents the upper part of the *Carcitanense* Subzone while KHA S04 correlates with the *Saxbii* Subzone. It should be noted that Gale et al. (1996) suggested that a *Schueteri* Subzone should be introduced in the *Mantelli* Zone between the *Carcitanense* zubzone

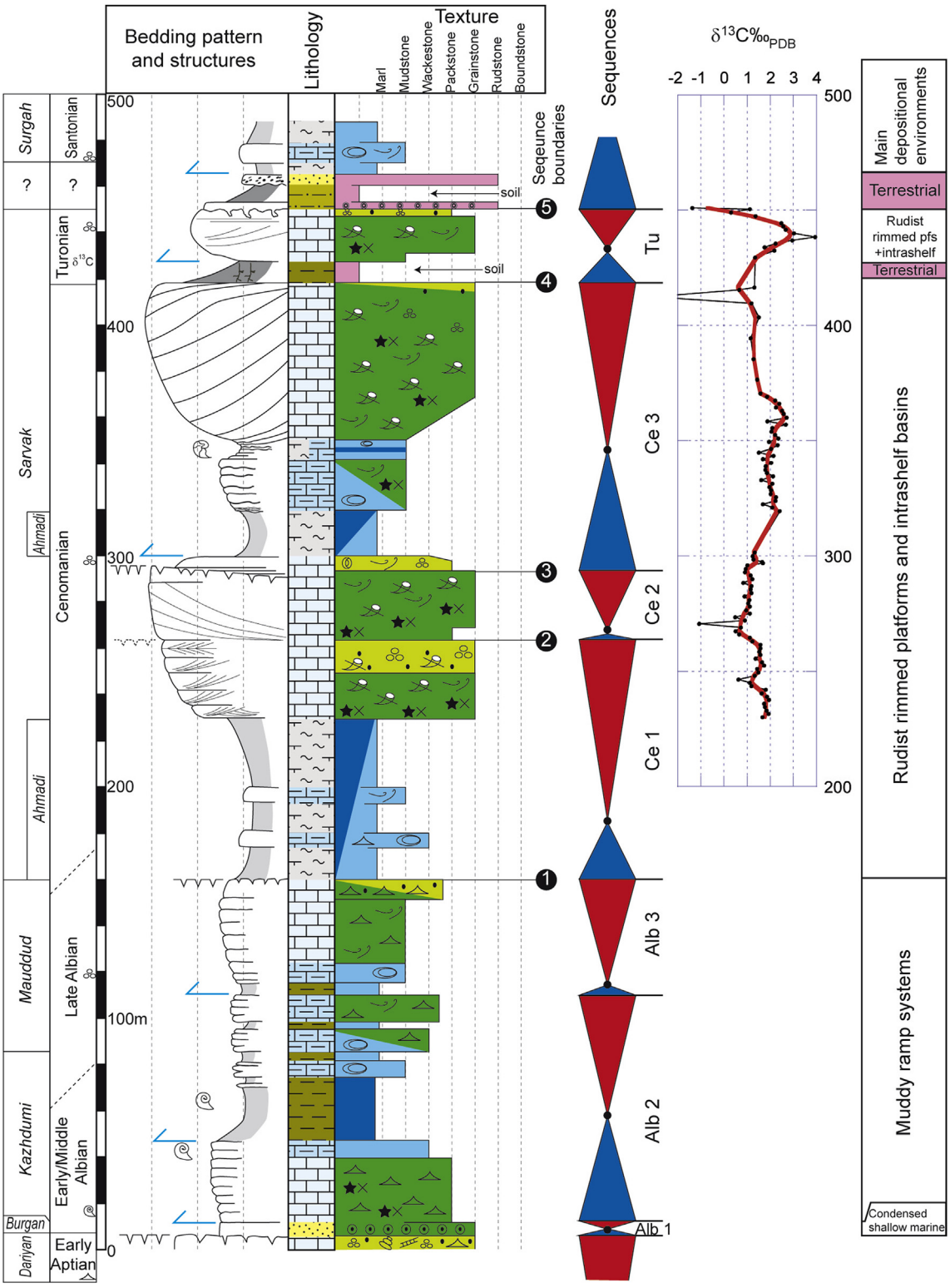

Figure 3. Sedimentological log of the Khormuj section, with sequence stratigraphic interpretation and bulk carbonate $\delta^{13}C$ curve (legend on Fig. 4).

and the *Saxbii* Subzone. This interval most likely correlates with the range of *Sharpeiceras schlueteri* at Khartang.

Orbitolinids were also used to date the lower part of the studied succession (Orbitolina Limestones and Kazhdumi Formation). These results were previously reported in Vincent et al. (2010a,b) and Schroeder et al. (2010).

Bulk $\delta^{13}C$ curves were constructed along the Khormuj, Asaluyeh, and Gach sections (Figs. 3, 5) to provide an independent correlation tool in addition to the biostratigraphic constraints. C isotope stratigraphy is very explicit in specific time intervals, such as the worldwide recognized C positive excursion associated with the Cenomanian–Turonian OAE (Oceanic Anoxic Event) 2 (*e.g.* Jenkyns,

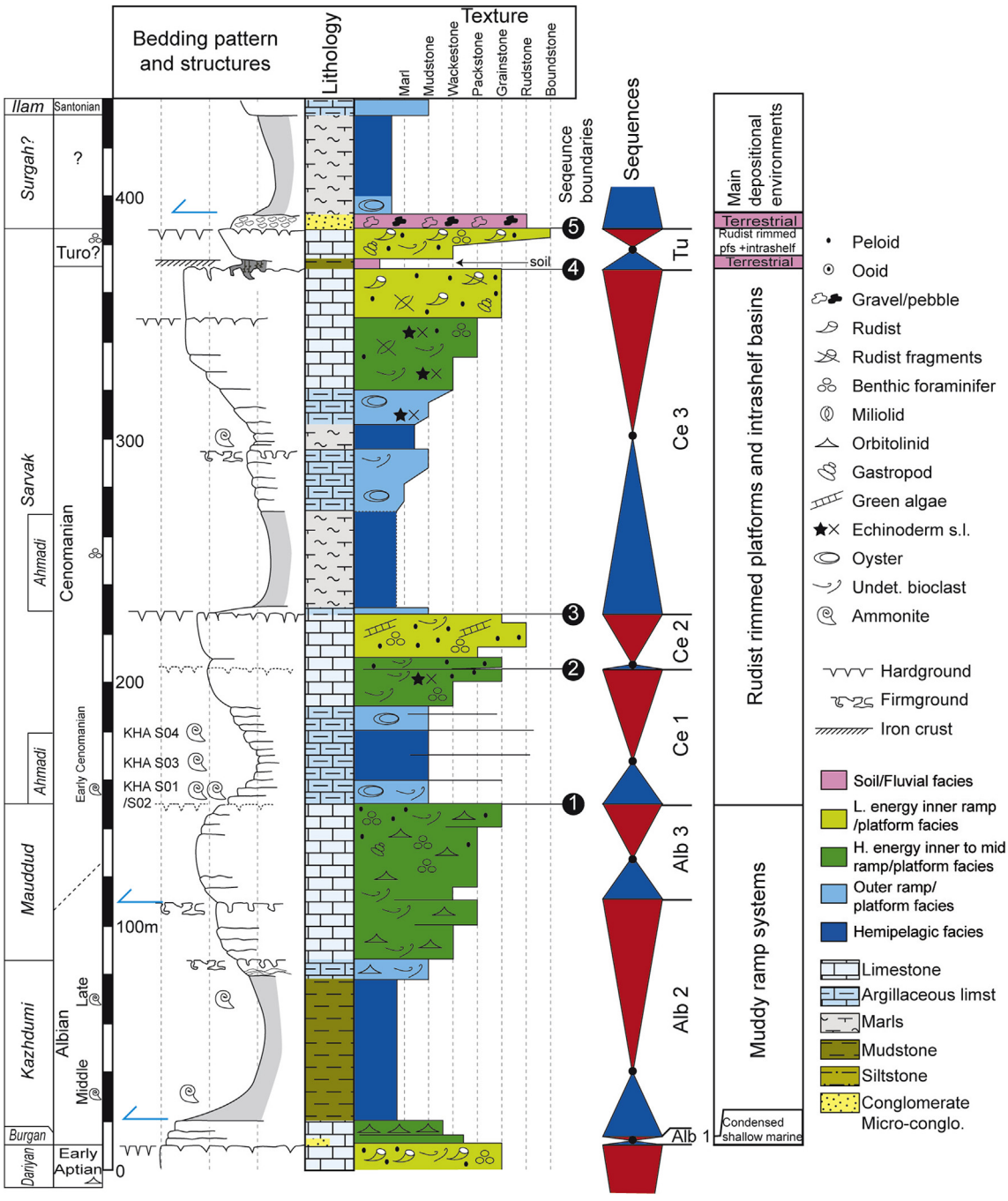

Figure 4. Sedimentological log of the Khartang section, with sequence stratigraphic interpretation and bulk carbonate $\delta^{13}C$ curve.

2010). The latter positive excursion is clearly identified in the upper part of the Khormuj (Fig. 3) and Gach (Fig. 5) sections. This is an element of correlation, locally and at the scale of the Arabian plate (*e.g.* Vahrenkamp, 2013), but not a direct accurate dating marker since the positive excursion extends from the Late Cenomanian to the Early Turonian (Elrick et al., 2009; Erba, 2004). Still, it bounds up the Sarvak Formation in an interval where indicative fauna are extremely rare.

4.2.2. Depositional sequences

A total of seven large-scale sequences are distinguished in the studied area, three in the Albian, three in the Cenomanian and one possibly of early Turonian age. Based on their duration they classify as 2nd and 3rd order sequences (*sensu* Vail et al., 1991). Detailed information about the individual stratigraphic sections is provided in Figures 3, 4, and 5, whereas regional correlations are shown in Figure 9. They are described hereafter.

The latest Aptian and Albian sequences are represented by the dominantly marly Kazhdumi Formation, which includes from base to top (1) the condensed iron-rich sandstones of the 'Burgan Sandstone equivalent' (*sensu* James and Wynd, 1965), (2) the Orbitolina Limestones, and (3) the limestones of the Mauddud Formation. The large scale sedimentological evolution of this interval starts with shallow water, orbitolinid-rich wackestone at the base to yellow/green marls of the Kazhdumi Formation in the middle, showing a gradual increase in carbonate rich beds

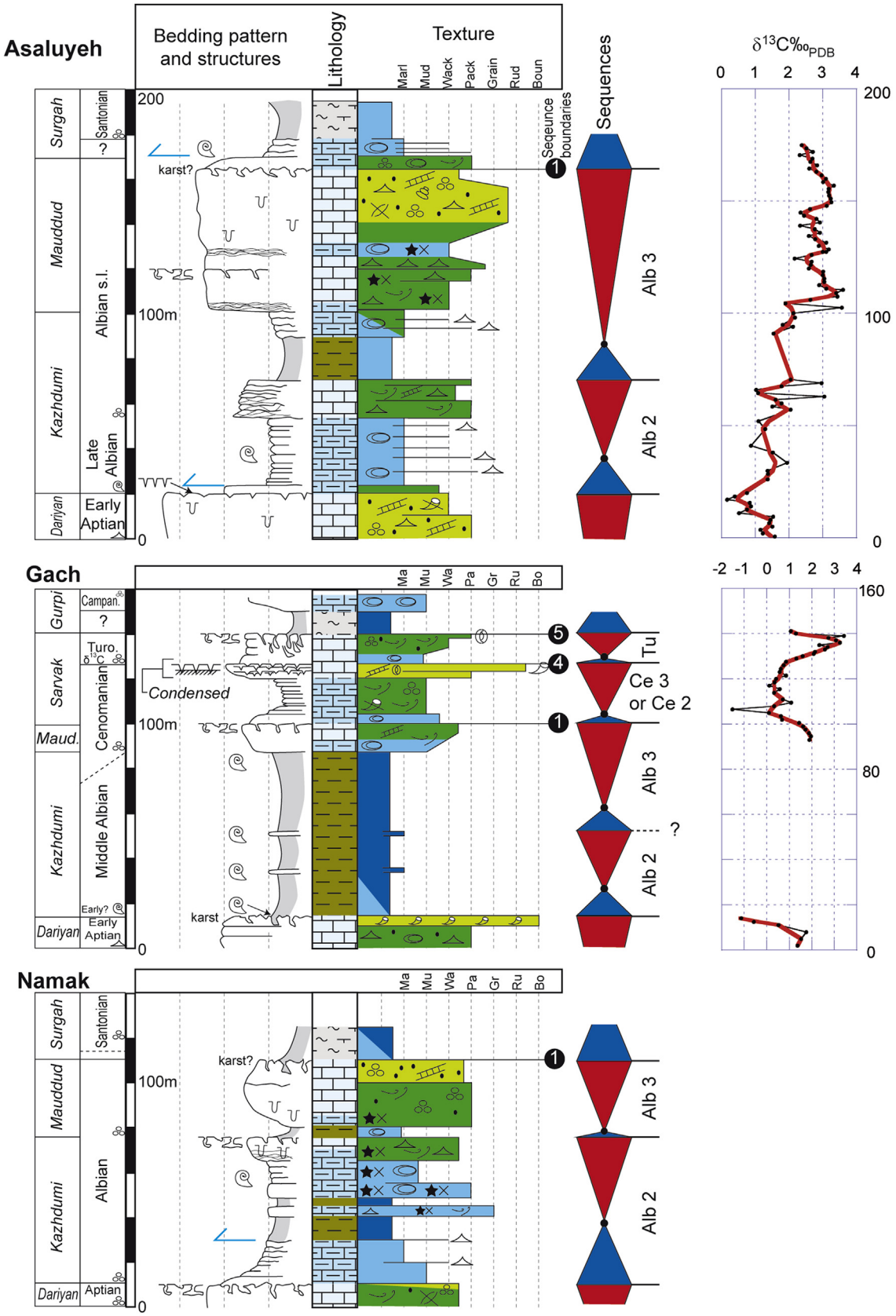

Figure 5. Sedimentological log of the Asaluyeh, Gach, and Namak sections, with sequence stratigraphic interpretation and bulk carbonate $\delta^{13}C$ curve (legend on Fig. 4).

Figure 6. Overviews of Khormuj (A), Khartang (B), and Namak (C) sections, with the positions of the main sequence boundaries.

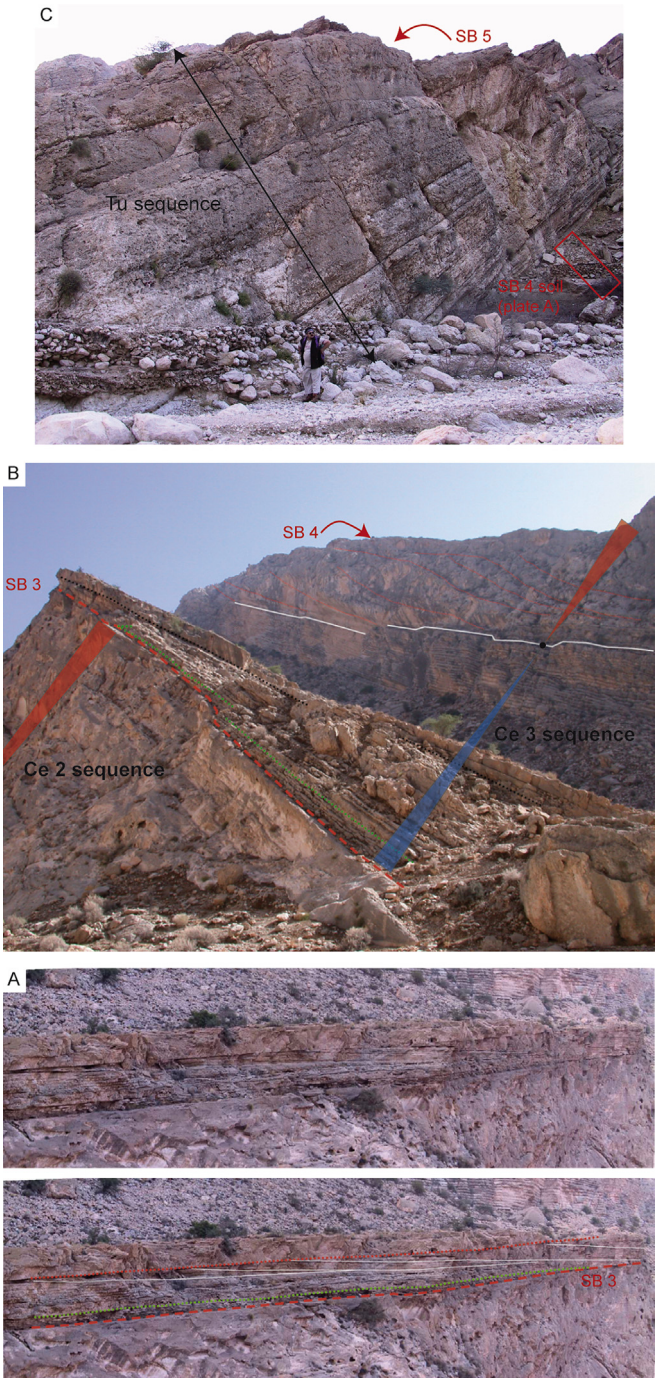

Figure 7. Remarquable sedimentary features and architectures in the Khormuj section. A – Onlaps of shallow marine carbonates above the SB 3 are later eroded (toplaps) by deeper marine carbonates B – Onlaps of shallow marine carbonates above the SB 3, and overview of the development of the sequence Ce-3 including the 80 m thick rudist-rich prograding wedge of the Sarvak platform. The downlap surface marks the MFS of the sequence Ce-3; C – Overview of the sequence Tu, bounded by two expositions described in detail in the text.

culminating in the muddy, orbitolinid and trocholinid-rich wackestone of the Mauddud Formation at the top. This overall evolution is very clearly expressed in the weathering pattern of these formations in the Khormuj section (Fig. 3). Within this overall evolution three large-scale depositional sequences are distinguished.

4.2.2.1. Latest Aptian/Early Albian (Alb-1) sequence. The basal unit of the studied interval is formed by the 'Burgan Sandstone equivalent', a 5 m-thick bed of iron-rich, locally glauconitic, siliciclastic deposits observed in the Khormuj and Khartang sections. In the other sections this sequence is absent and only represented by a hardground surface. The siliciclastic unit marks a sharp break with the carbonate sedimentation of the underlying Dariyan Formation, and is interpreted as a strongly condensed shallow marine deposit. No age dating is at present available for this unit.

Table 3
List of the stratigraphically significant ammonite fauna collected in the different sections with their stage and zone attributions.

Section	Sample	Species	Stage	Zone
Khormuj	KOJ 03A	*Knemiceras* cf. *syriacum* (intermediate form)	Middle Albian	
	KOJ 05	*Knemiceras* cf. *dubertreti*	Middle Albian	
Khartang	KHA 02B	*Oxytropidoceras* sp.	Middle Albian	
	KHA 04B	*Knemiceras* gr. *syriacum*	Late Albian	Cristatum
	KHA S01	*Utaturiceras* gr. *vicinale*	early Early Cenomanian	
	KHA S02	*Utaturiceras* gr. *vicinale*	early Early Cenomanian	
	KHA S03	*Utaturiceras* gr. *vicinale* *Sharpeiceras*	Early Cenomanian	
	KHA S04	*Sharpeiceras*	Early Cenomanian	
Namak	NAM V02	*Knemiceras syriacum*	Late Albian	Cristatum
	NAM V03c	*Knemiceras* gr. *uhligi*	Late Albian	Inflatum
	NAM V04	*Knemiceras uhligi*	Late Albian	Inflatum
	NAM V05	*Knemiceras uhligi*	Late Albian	Inflatum
Asaluyeh	ASL GB 05	*Knemiceras syriacum*	Late Albian	Cristatum
	ASL RS 01	*Knemiceras syriacum*	Late Albian	Cristatum
Gash	GASH 01	*Knemiceras persicum*	late Early Albian/early Middle Albian	Mammillatum/ Dentatus

A similar lithological unit in a comparable stratigraphic position has been observed offshore Qatar, where it is associated with the last phase of the siliciclastic infill of a large incised valley systems (Raven et al., 2010). Raven et al. (2010) and van Buchem et al. (2010) have interpreted this unit as a separate, strongly condensed sequence of latest Aptian/Early Albian age. In the absence of palynological age dating of the 'Burgan Sandstone equivalent', and based on the strong lithological resemblance and comparable stratigraphic position, both units are believed to be time equivalent, and thus of latest Aptian and earliest Albian age.

4.2.2.2. Middle/early Late Albian (Alb-2) sequence. The basal sequence boundary is formed by the top surface of the iron-rich sands, which is iron oxi/hydroxide-crusted, and shows no evidence for subaerial exposure. The upper sequence boundary is a slightly iron oxi/hydroxide-crusted surface topping an upward thickening trend of carbonate beds, and abruptly overlain by yellow/green marls. Uncertainty about the exact position of this boundary exists in the Gach section (Fig. 9).

A clear expression of the typical facies and bedding pattern evolution of this sequence is observed in the expanded Khormuj section (Figs. 3 and 6). The basal part is formed by orbitolinid-rich wackestone and packstone with occasional ammonites, overlain by green fossiliferous marls with large orbitolinids and ammonites, whereas in the upper part of the sequence thickening-up carbonate beds return. This sequence shows a variation in thickness from a maximum of 100 m in Khormuj (Fig. 3) to a minimum thickness of 50 m in Gach (Fig. 5).

Age control provided by the ammonites, shows that oldest units, of Early/Middle Albian age (*Knemiceras persicum* Collignon and *Knemiceras syriacum* von Buch), are represented by the Orbitolina Limestone units at the base in the Khormuj and Khartang sections, and a basal yellow/green marl unit in the Gach Section (Fig. 5). The basal sediments of this sequence in Assaluyeh have been dated as early Late Albian age (*Knemiceras syriacum* von Buch and *Knemiceras subcompressum* Hyatt). A regional onlap pattern onto the Qatar-Fars high is thus suggested. Whereby regional deposition of the yellow/green Kazhdumi marls was established in the region in the (Early part?) of the Late Albian (Fig. 9).

4.2.2.3. Late Albian (Alb-3) sequence. The basal sequence boundary is described above. The top sequence boundary is represented by the top surface of the Mauddud Formation (surface 1; Fig. 9). This surface has different expressions throughout the region, varying from an iron oxi/hydroxide-crusted surface, overlain by Ahmadi marls in the Khormuj and Khartang sections, to a weathered subaerial exposure surface representing a long hiatus (Cenomanian and Turonian) in Namak and Asaluyeh. Further details about this surface are provided below.

This sequence shows a lateral variation in facies. It is entirely carbonate dominated in the northern sections, whereas in the southern sections it is marly at the base and subsequently cleaning

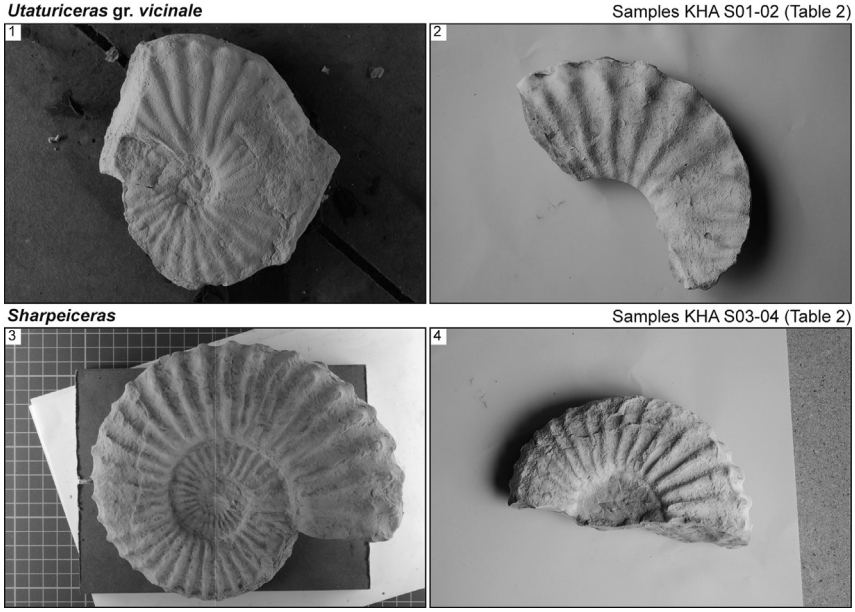

Figure 8. Stratigraphically significant ammonite fauna Photos 1/2: *Utaturiceras* gr. *vicinale* from the Khartang section, samples KHA S01-02 Photos 3/4: Sharpeoceras from the Khartang section, samples KHA S03-04.

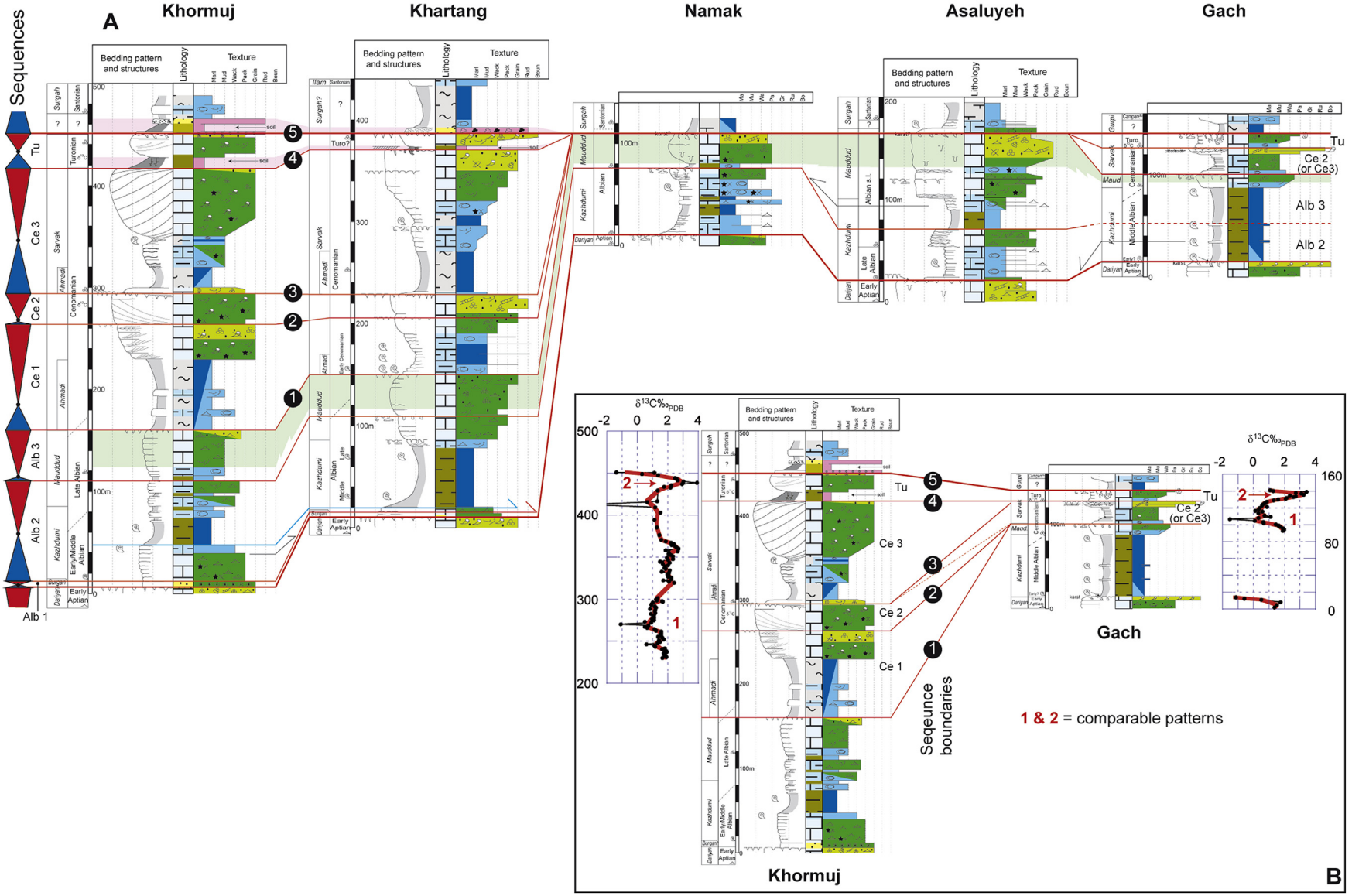

Figure 9. A – High resolution correlation between the 5 sections from the top Daryian Formation up to the top Sarvak Formation, *i.e.* from the Albian to the Turonian. Noteworthy is the relative continuity of the Mauddud platform in the sequence Ce 1 over the panel, whereas the Cenomanian Sarvak-related sequences are absent on the axis of the Qatar-Fars high (Namak and Asaluyeh). B – Correlation between the two external sections of the transect, Khormuj and Gach, supported by bulk $\delta^{13}C$ curves. Despite variable sedimentation rate, comparable patterns are observed in the $\delta^{13}C$ curves on each side of the arc.

up to a carbonate facies. A typical element of the carbonate facies is the high concentration of the orbitolinid and trocholinid benthic foraminifers. A decimeter to meter scale horizontal bedding is observed, but no cross-bedding. This sequence varies in thickness from 50 m in Khormuj, to 95 m in Asaluyeh, and 30 m in Namak. The overall depositional model is a low-angle muddy ramp.

The age of this sequence is interpreted as middle Late Albian to late Late Albian, which is based on the ammonites found below and above this sequence (see detailed information provided in the biostratigraphy section above).

The Cenomanian/Turonian rocks are represented by the middle and upper part of the Sarvak Formation. Three Cenomanian sequences and one possibly Early Turonian sequence are distinguished. These are well preserved in the Khormuj and Khartang area, which is used as reference, while they are poorly preserved in the Gach section, and entirely absent in the Asaluyeh and Namak sections (Fig. 9).

4.2.2.4. Early Cenomanian sequence (Ce-1). The basal sequence boundary corresponds to the top surface of the Mauddud Formation (surface 1) and is described above. The top sequence boundary (surface 2; Fig. 9) is expressed as a facies change, locally overlaying a hardground.

The Khormuj and Khartang sections show a very similar facies succession, starting with a marly, fossiliferous (ammonite-rich in the case of Khartang) facies at the base, evolving into grainstone and packstone, locally with cross-beddings (in Khormuj, with decimeter bedsets), in the upper part of the sequence. This evolution is interpreted as an overall shallowing-up trend from a muddy intrashelf basin setting to a grainy shallow water carbonate platform setting. Regionally, this sequence shows significant variations in thickness, ranging from approximately 100 m in the Khormuj and Khartang area, to complete absence in the nearby Namak and Asaluyeh sections.

The age of this sequence is Early Cenomanian based on the ammonite fauna present in the Khartang section (see above).

4.2.2.5. Middle Cenomanian sequence (Ce-2). The basal sequence boundary is described above. The upper sequence boundary (surface 3) is erosional and marks a sharp facies change in the Khormuj section, and is a hardground also marking a sharp facies change in the Khartang section (Fig. 4).

In Khormuj, the facies is a coarse grainstone with steep-angled, tangential cross-bedding and a depositional relief in the order of 25 m. In nearby Khartang no large scale cross-bedding was observed, and the succession is slightly thinner and muddier too, suggesting a more internal, intra-platform setting.

Correlation with the Gach section is uncertain. A 25 m thick unit of marls and limestones is present above the Mauddud Formation (Fig. 5) of which the exact biostratigraphic attribution is uncertain, microfossils giving a broad Cenomanian age. However, low $\delta^{13}C$ values between +0.5‰ and +1‰, with a negative isolated data (−1.5‰) located in the trangressive facies (Figs. 5, 9) are recorded in this unit. A very similar $\delta^{13}C$ pattern characterizes the Ce-2 sequence in the Khormuj section where $\delta^{13}C$ values also range between +0.5‰ and +1‰ with a negative point (−1.1‰) also located in the transgressive phase (Figs. 3, 9). This similarity may indicate a contemporaneous deposition. Understanding the origin of such low $\delta^{13}C$ value above sequence boundaries in transgressive facies is far beyond the scope of this work. However, reducing conditions in the transgressive interval are attested in the Gach section by the presence of pyrite, and one could easily imagine an input of $\delta^{13}C$ depleted carbonate generated as a by-product of sulfate reduction (*e.g.* Dickson et al., 2008). Another explanation could be the input of ^{12}C-rich carbonate ions from microbial degradation of organic matter, often present in the transgressive argillaceous facies in the area (unpublished data).

4.2.2.6. Late Cenomanian sequence (Ce-3). The basal sequence boundary is described above. The top sequence boundary (surface 4) is a distinctly developed subaerial exposure surface, except in the Gach section where it corresponds to stacked hardgrounds and iron crusts (Fig. 5). It is described more in depth in the next section.

The sequence boundary is overlain and onlapped by a 10 m thick unit of channelized shallow-marine, miliolid-rich packstone, which are subsequently truncated by the overlying intrashelf basinal facies (Fig. 7). A well-developed interval of deeper marine intrashelf basinal facies represents the trangressive systems tract in both the Khormuj and Khartang sections (Figs. 3, 4). The upper part of the sequence is represented in the Khormuj section by a spectacular 90 m thick, rudist-rich unit of prograding clinoforms. These are interpreted as the coarse grained margin of the carbonate platform, and suggest that the intrashelf basin was at least 90 m deep (Fig. 7). In the Khartang section, the sequence has a comparable thickness, but here no evidence for large scale clinoforms have been observed. In contrast, the succession is characterized by decimeter and meter-scale horizontal bedding and shows an overall coarsening upward trend. The environment is interpreted as a more internal platform setting.

This sequence is inferred to be of Late Cenomanian age.

4.2.2.7. Early (?) Turonian sequence (Tu-1). The top sequence boundary (surface 5) is a distinctly developed subaerial exposure surface, except in the Gach section, where it only appears as an intensively bioturbated surface (Fig. 5). From a geochemical point of view, in both Khormuj and Gach sections, the positive $\delta^{13}C$ peak of the OAE2 is followed by a sharp shift to lighter values (Figs. 3, 5). The top surface is further described in the next section.

The sequence starts with a package of paleosoils, which is 4 m thick in the Khormuj area, and 1 m thick in the Khartang section (Figs. 3, 4, 9). This is overlain by open marine carbonates, marking a relative rise in sea level.

Based on the biostratigraphic attribution of Wynd (1965) a possible Turonian age is suggested for this sequence in both Khormuj and Khartang. Supporting evidence for this age comes from the bulk $\delta^{13}C$ curve of the Khormuj section, which shows a remarkable consistent positive peak in the shallow-marine carbonates above the paleosoil reaching about +4‰ (Fig. 3). Such high values were reported all around the world, characterizing the OAE2 event, but again tend to extend between the Late Cenomanian and the Early Turonian. In the Gach section, a 10 m thick unit is tentatively attributed to the Tu-1 sequence (Figs. 5, 9). The biostratigraphic attribution is uncertain but a Turonian age is possible. The $\delta^{13}C$ curve shows, a consistent positive peak up to about +3.5‰ in the shallow-marine carbonates of the regressive part of the sequence, a very similar pattern to what is observed in Khormuj section (Figs. 5, 9).

4.2.2.8. Mid Turonian/Coniacian exposure and Santonian flooding. The top boundary of Tu-1 sequence is overlain in the Khormuj section by a pluri-meter thick paleosoil package which contains fluvial micro-conglomerates and pisoliths (Fig. 4 and see below), and in the Khartang section by a 4 m thick conglomerate (Fig. 4). These deposits are abruptly overlain by deep marine marls and argillaceous limestone with oysters and planktonic foraminifers of the Surgah Formation. The first dated beds above the flooding are of Santonian age. A similar transgression is observed in the Gach section, but here the overlaying marls are of Campanian age (Gurpi Formation; Fig. 9). This means that at least most of the Turonian and the Coniacian are absent, or extremely condensed in

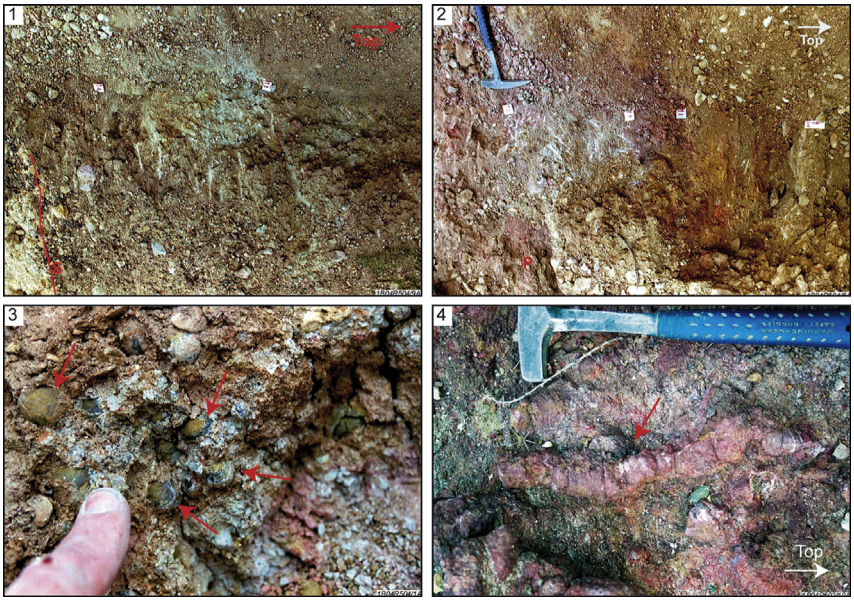

Figure 10. Khormuj section – late Cenomanian paleosoil sequence associated with the SB4 Photo 1: Lower part of paleosoil sequence. Note the olive gray dominant color. Photo 2: Upper part of the paleosoil sequence, with a pisoid-rich level (P, below the dashed black line). Note the red dominant color. Photo 3: Detail of the iron pisoid-rich layer in the paleosoil sequence. Photo 4: Subvertical tube-like cemented feature (arrow) interpreted as fossilized roots. (For interpretation of the references to colour in this figure legend, the reader is referred to the web version of this article.)

dominantly continental deposits, on the northwestern flank of the Qatar-Fars high (Khormuj and Khartang), which corresponds to a hiatus of at least 3 Ma. On the southeastern flank (Gach) the hiatus includes the Santonian, suggesting a non-deposition and/or condensation of at least 7 Ma.

On the axis of the Qatar-Fars high, the stratigraphic record is even less complete. In both Namak and Asaluyeh sections, all the Cenomanian and Turonian sequences are absent, and all the sequence boundaries from 1 to 5 are stacked at the top of the Mauddud (Figs. 5, 9). The late Albian shallow-marine carbonates of the latter formation are immediately capped by deep water argillaceous limestone with planktonic foraminifers giving a Santonian age (Fig. 5). This represents a hiatus of at least 13Ma.

5. Expressions of sequence boundaries

In this section the diagenetic expression of two of the above defined sequence boundaries is presented in detail. These have been chosen for the presence of clear evidence for subaerial exposure and their importance in understanding the overall evolution of the depositional system.

They were studied in detail in the Khormuj section where they are best expressed and easily accessible. Additional observations were made in several other sections, however in these locations the expression was more subdued, and has less clear sedimentological, petrographic, or geochemical expression.

5.1. Surface 4: top Ce-3 sequence boundary (Sarvak Formation)

The Cenomanian 3 Sequence is overlain by a several meter thick interval of fine grained siliciclastics in the Khormuj section (Fig. 3). The succession is composed of 4 units and develops above a 25 cm thick transition zone beginning with severely altered limestone and ending with nodules of chalky limestone floating in a clay matrix. The first unit corresponds to a 2.05 m thick bed of olive gray clays with minor amount of silt (Fig. 10, photo 1). The second unit is a 25–30 cm thick pisoid-rich red to brick-red colored layer (Fig. 10, photos 2, 3), overlain by a third unit of 25–30 cm thick olive green gray clayey silt. The last unit corresponds to a 1 m thick silty clay interval with a mottled color distribution becoming more consistently red to brick-red to the top (Fig. 10, photo 2). Some subvertical calcified features are interpreted as root traces also occur in this overall interval (Fig. 10, photo 4). Five samples were taken for clay fraction analysis, and all of them with the exception of the sample taken in the upper meter contain only kaolinite. The uppermost sample is still dominated by kaolinite but also revealed traces of illite and smectite.

This thick siliciclastic succession is interpreted as evidence for a major period of soil development, alternating colors reflecting oxygenated vs. reducing conditions, with possibly the superposition of several paleosoils. The almost exclusive kaolinite mineralogy is indicative of a tropical weathering profile, causing the formation of authigenic clay minerals as alteration product of weathered aluminum-silicates (*e.g.* Chamley, 1989). While the topmost 2 samples of the underlying sequence display slightly depleted bulk $\delta^{13}C$, one sample taken about 4 m below the paleosoil contact displays a very negative value (−2.89‰; Fig. 3). This probably illustrates a heterogeneous recrystallization of the limestone below the top surface involving light carbon from the soil zone CO_2 (*e.g.* Allan and Matthews, 1982; Joachimsky, 1994).

In the Khartang section, the same stratigraphic interval corresponds to a 1 m thick of red to brick red clays overlying the iron oxi/hydroxide-crusted top surface of the underlying sequence (Fig. 11, photos, 1, 2).

In the Gach section, this sequence boundary is more difficult to place with accuracy, since several iron oxi/hydroxide-crusted surfaces and 3 purple-stained hardgrounds are stacked in a 3 m thick rudist-rich boundstone bedset (Fig. 11, photo 7). The surfaces 3 and 4 are stacked within the following succession:

- a 40 cm thick rudist boundstone immediately overlays a first hardground. It is itself overlain by a 40 cm thick coralgal boundstone, without well-expressed surface between the two layers. The uppermost 10 cm of the unit correspond to a shell-

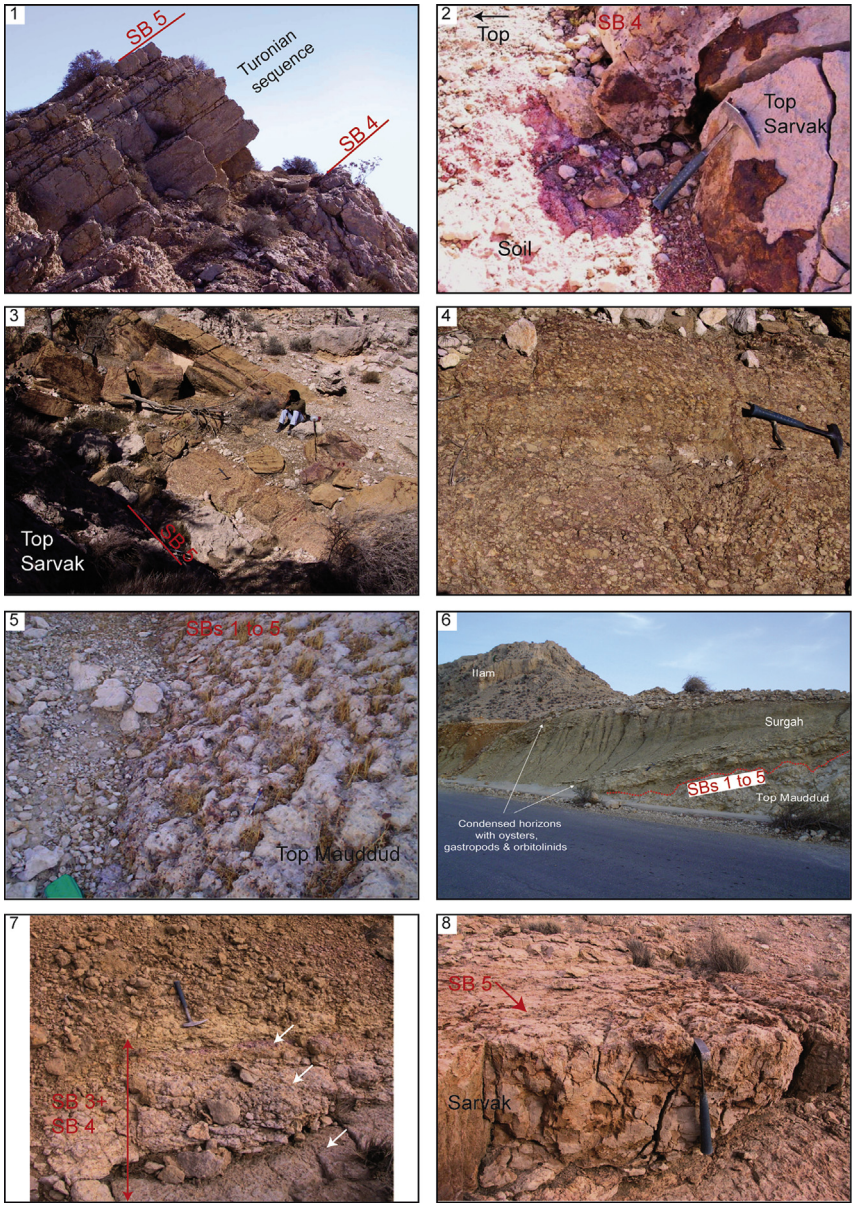

Figure 11. Expression of the main sequences boundaries in Khartang, Namak, Asaluyeh, and Gach sections Photo 1: Khartang section – Sequence Tu bounded by SB 4 and SB 5. Photo 2: Khartang section – Overview of the red paleosoil developed above at the SB 4 above the top Ce 3 sequence. Note the thick oxidized iron crust capping the limestone. Photo 3: Khartang section – Thick fluvial conglomerate unit above the SB 5 and the top Sarvak. Photo 4: Khartang section – Detail on the Fe oxi-hydroxide-rich polygenic conglomerate with faint cross-bedding. Photo 5: Namak section – Top Mauddud surface stacking SB 1 to 5. The pitted aspect illustrates either a weakly evolved epikarst or a simple bioturbated surface. Photo 6: Asaluyeh section – Top Mauddud surface stacking SB 1 to 5. The surface is irregular and the limestone are intensively chalkified. Photo 7: Gach section – Condensed interval with 3–4 purple stained hardgrounds in rudist boundstone, corresponding to the stack of SB 3 and SB 4. Photo 8: Gach section – Sharp top Sarvak surface, *i.e.* SB 5. It consists of a simple bioturbated surface on top of shallow-marine carbonates. (For interpretation of the references to colour in this figure legend, the reader is referred to the web version of this article.)

and algae-rich packstone capped by a hardground which displays abundant borings, filled with overlying grainy material,

- a new coralgal boundstone with a thickness of 40 cm develops above. It is capped by a purple hardground also displaying abundant perforations,
- laying on the previous hardground, another 60 cm thick rudist boundstone is present. The top of this boundstone consists of a Fe crust,
- a 90 cm thick miliolid-rich grainstone overlays the crust. No surface has been distinguished on the top of this grainstone which is overlain by a last rudist boundstone of 40 cm thick. This boundstone is capped by a third purple hardground, very similar to the previous.

Noteworthy is the absence of significant rudist dissolution, as well as the consistent low but positive and increasing bulk $\delta^{13}C$ values in this interval (Fig. 5). Despite any petrographic investigation was made in this zone, these observations may indicate the absence of exposure and continuous marine conditions.

5.2. Surface 5: top Tu-1 sequence boundary

The top of the Sarvak platform displays another complex succession in the Khormuj section illustrated in Figure 12. Above intensively altered rudist-rich limestone, this succession is composed of two main sets: (1) a layer of variegated red brown

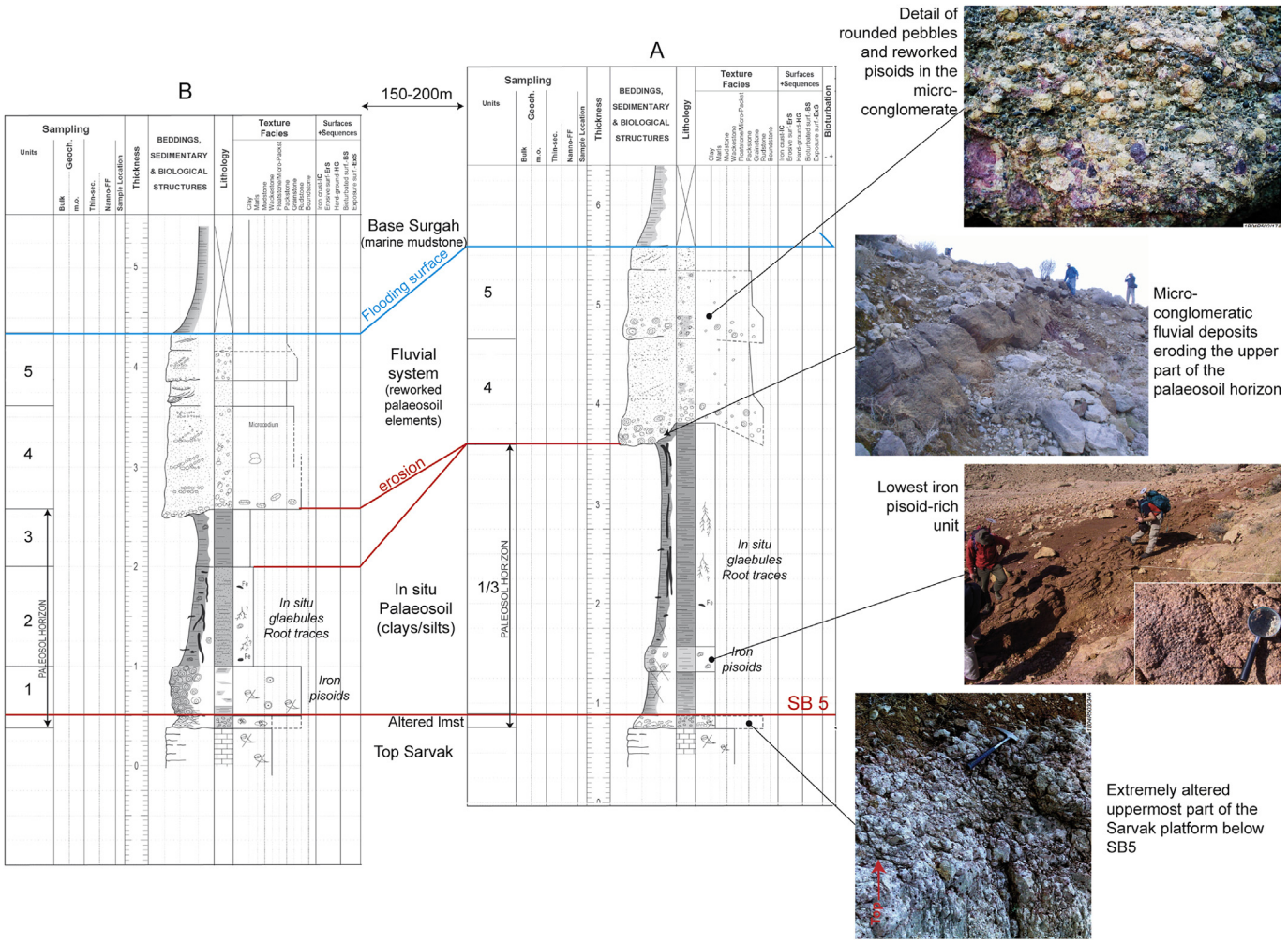

Figure 12. Correlation between 2 high resolution logs of the continental succession at SB 5 in the Khormuj section. The micro-conglomeratic unit is clearly erosive and removed variable thickness of the underlying soil sequence.

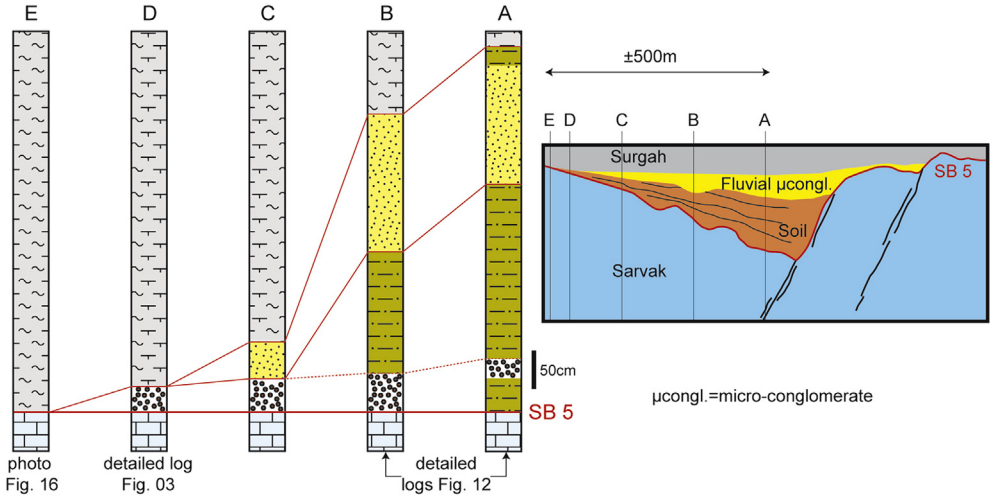

Figure 13. Simplified sketch explaining the differential record of the paleosoil sequence and the micro-conglomerates at the SB 5, *i.e.* the Middle Turonian Unconformity of Sharland et al. (2001). Early faulting observed in the field created some depressions were the entire continental succession is best preserved. However, soil development occurred everywhere prior to faulting (see explanation in the text).

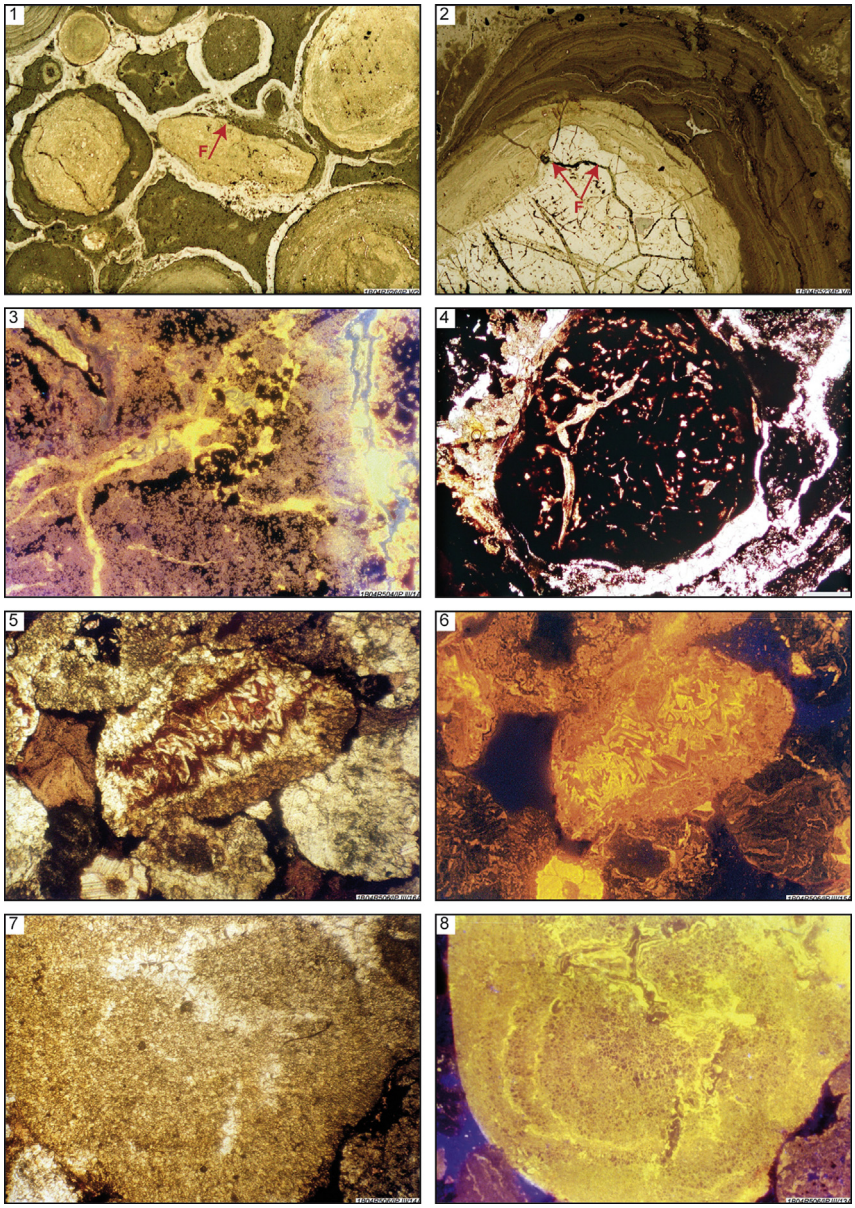

Figure 14. Khormuj Turonian (SB 5) paleosoil micro-photographs Photos 1/2: Incident light microphotographs illustrating: the complexity of the pisoid internal nature, the complex zonation patterns, the difference in crystallinity of the Fe oxi/hydroxides reflected in the difference of reflectance, as well as the way the different pisoids are glued together. Note the internal early micro-fractures (F) and reworking features on the pisoids. Photo 3: Detail of internal cracks/micro-fractures inside pisoids under cathodoluminescence (CL). The cracks are cemented by a zoned bright luminescent calcite. Photo 4: Opaque Fe oxi/hydroxide-rich "pseudo-nodules" of which some are fractured. Photos 5/6 (PL, polarized light/CL): Sparitic pebbles in the micro-conglomerate. The central one possesses a nicely zoned luminescence fabric. Zonations are cut at the fragment edges illustrating an early erosion and transport. Photos 7/8 (PL/CL): Microsparitic brown to bright luminescent pebble with zoned bright yellow calcite cemented cracks. These pebbles may be interpreted as crystallaria. (For interpretation of the references to colour in this figure legend, the reader is referred to the web version of this article.)

colored clays with locally the presence of pisoid-rich levels especially at the base of the layer, (2) a bed of conglomerate reworking pebbles from the underlying clays and altered Sarvak limestone. The latter coarse grained bed shows an erosive basal contact with the underlying clays which consequently display a variable thickness (Fig. 12). Locally the conglomerates immediately lie on the pisoids just above the Sarvak limestone (Fig. 13). On the contrary, the clay layer is particularly well developed and/or preserved in fault-related depressions, which directly indicates a period of significant tectonic activity (Fig. 13).

A high resolution study of the siliciclastic succession reveals 5 main units (Fig. 12). Above a layer of clay-rich nodular limestone, the unit 1 corresponds to beige colored clays (>50 cm thick), generally devoid of carbonate components, with pisoids. Very locally some coarse crystalline rudist relicts occur in this lithology. The following dark red to brick red clay–silt unit 2 (80–120 cm thick), sometimes displays Fe oxi/hydroxide concretionary features. The latter locally display tube-like outline resembling root features. Within the matrix locally some irregular Fe oxy/hydroxide clasts/nodules are floating. They sometimes are composite, *i.e.* clast in clast, sometimes with the development of real pisoids (Fig. 14, photos 1, 2). The impression arises here that this could be a product of a kind of ferralitisation/bauxitisation process. Locally some small pebbles, less than 2 cm in length are floating in the matrix. Typical are the presence of zoned bright luminescent calcite cemented cracks inside and around the pebbles and pisoids (Fig. 14,

photo 3). Pisoids and pebbles are surrounded by circumgranular calcite-filed cracks (Fig. 14, photos 1, 2). Furthermore some fractures occur with slickenslide-like features. Whether the latter relate to pedogenesis is unclear. The unit 3 is similar to the previous unit but is less reddish colored, and more homogeneous (30 cm thick, at maximum). This unit is locally eroded by the overlying coarse grained deposits (Fig. 12). Here some "pseudo-nodules" occur with, in the center, some pisoid-like structures surrounded by a Fe oxi/hydroxide rim and some white colored material. In thin-section most of the "pseudo-nodules" are opaque (Fig. 14, photo 4). Under cathodoluminescence they are either bright or dull luminescent.

Unit 4 corresponds to the first bed of the coarse grained succession. It is a micro-conglomeratic unit (up to 120 cm thick) consisting of flat to irregularly rounded, sometimes aligned pebbles (Fig. 12). They are somewhat elongated, 2 cm in length and maximum 1 cm in diameter. The term "pebbles" is used here to describe reworked and transported clasts, which are very comparable to the clasts described in the previous units, however the latter seem to have been formed in situ. Pisoids are also common at the base of this unit. The pebble alignment gives rise to some faint cross-bedding as well as some parallel bedding. Locally imbrication features between pebbles occur as well as pebbles incision structures between individual sets. Some calcite cement has been recognized filling the former interparticle pore-space, but the matrix between the pebbles consists of red clay in the uppermost part of the unit. In thin section different type of pebbles can be recognized: (1) microsparitic dull luminescent, dark brown semi-to non-transparant pebbles which are crosscut with nicely zoned often bright luminescent calcite cracks, (2) sparitic pebbles with nicely zoned luminescence fabric, however which clearly have been eroded and transported since the zonations are cut at the fragment edges (Fig. 14, photos 5, 6), (3) micritic/microsparitic brown to bright luminescent with calcite cemented cracks resembling crystallaria (Fig. 14, photos 7, 8). Especially noteworthy is that bright yellow zoned luminescent pebbles regularly occur next to dull luminescent pebbles, illustrating the high degree of mixing of the different pebbles. Some of these pebbles seem to consist of carbonate mudstone with faint cracks and thus could correspond to glaebules (*e.g.* Allen, 1986). Above this thick bed, the unit 5 consists of more thin-bedded poorly sorted micro-conglomerates, with some cross-bedded "pebble-stone" with faint channel-type incisions (Fig. 12).

Units 1 to 3 are interpreted as remains of a paleosoil horizon. This is mainly based on the presence of glaebules with

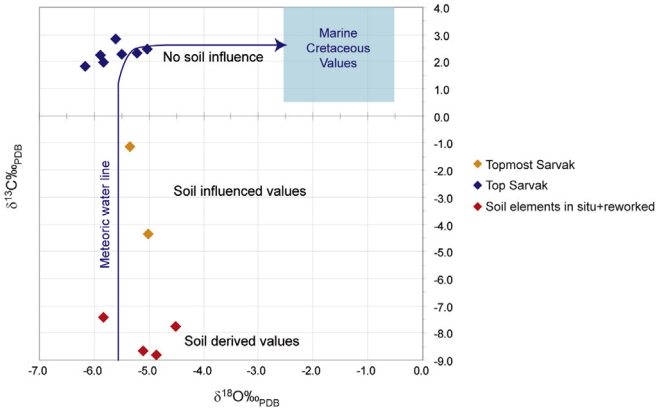

Figure 15. $\delta^{18}O/\delta^{13}C$ cross-plot of the SB 5 soil elements and some carbonates of the uppermost Sarvak Sequence Tu in the Khormuj section. Note the classical fast carbon rock-buffering compared to oxygen along a meteoric water line.

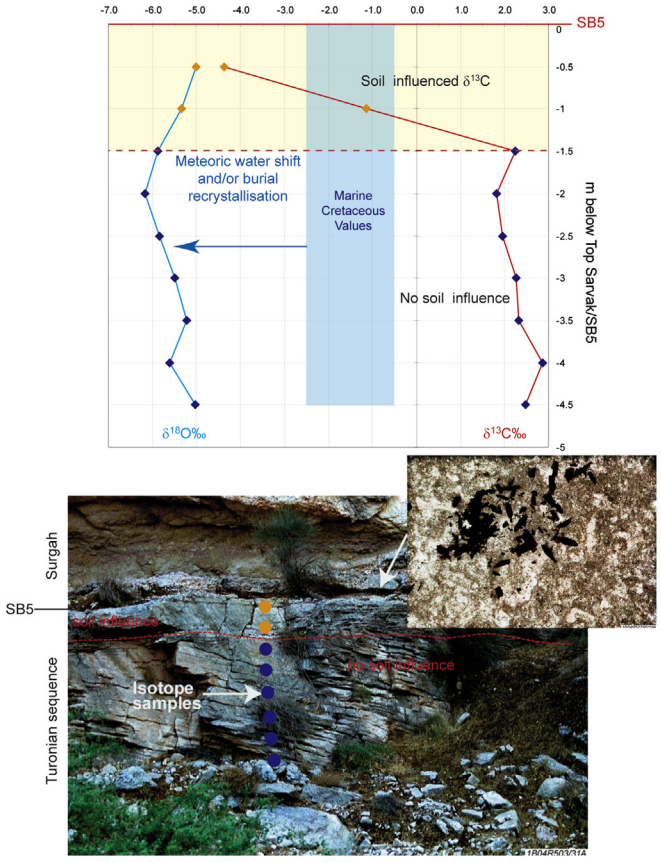

Figure 16. Stable isotope profiles in topmost Sarvak limestone, below the SB 5 in the Khormuj section. Noteworthy is the absence of continental deposits (paleosoil, micro-conglomerates) above the extremely recrystallized Sarvak limestone (thin section photo), immediately overlain by Surgah marls/argillaceous limestone. Despite this absence clear soil evidence is visible on the $\delta^{13}C$ profile (see the text for further explanation).

circumgranular cracks and crystallaria (*e.g.* Sehgal and Stoops, 1972), as well as the existence of root-like features. In order to confirm the pedogenetic nature of the in situ "pseudo-nodules" in unit 3, which are comparable to the ones present in the lower units, one "pseudo-nodule" was analyzed with regard to its stable carbon and oxygen isotopic composition. The $\delta^{13}C$ signature of −7.76‰ is in line with a pedogenetic origin whereby the depleted signature points to involvement of soil-derived CO_2. The units 4 and 5 are interpreted as subaerial fluvial deposits of products of soil erosion, where glaebules and other weathering products from former soils are reworked. Noteworthy is the virtual absence of quartz grains in these units, supporting the weathering of carbonate dominated lithologies in the hinterland. Different pebbles were analyzed with regard to their stable carbon and oxygen isotopic composition (Fig. 15). The $\delta^{13}C$ of these pebbles varied from −8.82 to −7.41‰. This signature is clearly in line with a pedogenetic origin whereby the depleted signature, as already mentioned above, points to involvement of soil derived CO_2. Also the $\delta^{18}O$ signature with values of −4.87 to −5.83‰ points to involvement of meteoric water, as for the in-situ pseudo-nodule (Fig. 15).

In an attempt to infer whether the limestone below the sequence boundary corresponding to the surface 5 were affected by processes in relation to exposure and paleosoil development, plugs sampled every 50 cm over an interval of 5 m, were analyzed for stable isotope analysis (Fig. 16). Notice that on the selected profile the Sarvak limestone is not covered by a paleosoil, the Surgah deposits starting immediately above the Sarvak altered limestone

(Figs. 13, 16). The $\delta^{18}O$ in the sampled limestone varies between −5‰ and −6.2‰, which compared with Turonian marine signatures (*e.g.* Veizer et al., 1999) clearly is depleted. The most likely explanation is that the limestone recrystallized due to the infiltration of meteoric water; indeed the top Sarvak microfacies is extremely crystalline, and identifying allochems is almost impossible. However, considering the tectonic history of the Zagros range, similar oxygen isotope values and petrographic characteristics could reflect "simple" recrystallization during burial. The $\delta^{13}C$ of the limestone below 1 m−1.5 m away from the top surface vary between +1.8‰ and +3.0‰ (Fig. 16). The latter are in line with the early Turonian marine signature (*e.g.* Veizer et al., 1999), and thus indicate that despite a strong recrystallization, the $\delta^{13}C$ signature of the limestone was not affected. However the $\delta^{13}C$ signature in the uppermost 1 m of limestone is clearly depleted (<−1‰; Fig. 16). The latter can best be explained by the infiltration of soil derived CO2 (*e.g.* Allan and Matthews, 1982; Joachimsky, 1994). Despite the absence of conclusive field evidences of paleosoil development in the studied profile (Fig. 16), stable isotope recorded the existence of paleosoil(s) at the top Sarvak, which has been eroded prior to the deposition of later deep marine sediments. A similar abrupt shift to light $\delta^{13}C$ values is also observed in the bulk $\delta^{13}C$ curve (Fig. 3), which samples come from a profile with a well-developed paleosoil sequence. This means that the structuration of the top Sarvak occurred after the development of a continuous continental succession, at least at a local scale.

In the Khartang section, also on the northern flank of the Qatar-Fars high, the outcrop quality did not allow to study the top Sarvak zone in detail. However, there is no evidence of paleosoil above the top Sarvak, which is quite sharp and much less recrystallized than in Khormuj (*i.e.* allochems are clearly recognizable). Above the shallow-marine limestone, a 4 m thick Fe oxi/hydroxide-rich polygenic conglomerate with faint cross-bedding shows mud clasts, reworked pisoids, and reworked fragments of shallow-marine limestone (Fig. 11, photos, 3, 4). This conglomerate is interpreted as a fluvial to fluvio-deltaic deposit.

In the Gach section, the Turonian unconformity is less well-expressed despite it represents a longer gap in sedimentation. A sharp contact between bioturbated (*Thalassinoides* burrows) shallow-marine limestone and planktonic foraminifer-rich marls illustrates a rapid flood in a continuously marine environment (Fig. 11, photo, 8). Neither karst nor paleosoil evidence were observed, but a shift to lighter $\delta^{13}C$ values, not negative (around +1‰), nevertheless does occur below the surface (Fig. 5). While the shift to negative $\delta^{13}C$ values is related to the exposure-related diagenesis alteration in Khormuj, the downward shift in the Gach section may be an effect of early marine diagenetic processes as described by Dickson et al. (2008). However, this shift could also illustrate the worldwide recorded decrease of the $\delta^{13}C$ marine signal in the Turonian after the OAE2 event (*e.g.* Elrick et al., 2008).

In the Asaluyeh section, the Turonian unconformity corresponds to the stack of the surfaces 1 to 5 and represents a more than 10Ma hiatus, but it only appears as an irregular erosive surface (Fig. 11, Photo 6) which could be interpreted as a weakly developed epikarst. However, apart a strong alteration ("chalkification") of the underlying limestone, no real evidence of karst (abundant vugs, caves, geopetal silts,...) or long lasted exposure was observed. Moreover, the bulk $\delta^{13}C$ curve does not show any apparent alteration except a slight decrease in the 10 uppermost meters below the surface (Fig. 5).

In the Namak section, the same >10 Ma hiatus (surfaces 1–5) corresponds to a sharper surface however displaying a pitted aspect (Fig. 11, Photo 5), and which could either be a weakly evolved epikarst, or more simply a bioturbated surface. Some biomolds are

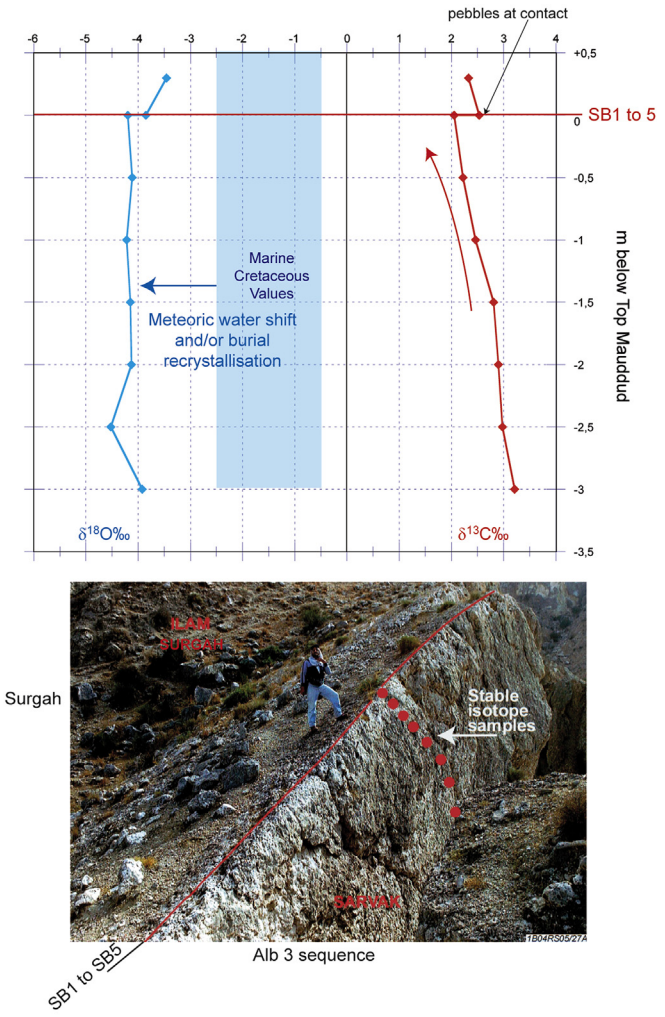

Figure 17. Stable isotope profiles in topmost Mauddud limestone, below the SB 1-5 in the Namak section. Any macroscopic exposure evidence was observed in the field, and no clear isotopic evidence neither, except possibly the continuous slight upward decrease of the $\delta^{13}C$ (see the text for further explanation).

present, but not significantly enlarged, which is not a clear evidence for an exposure on top. More critical is the patchy erratic distribution of chalky to tight limestone in the top 30 m of the Mauddud Formation. Such a pattern could reflect a possible karst-related alteration. Similarly to what was done in Khormuj, plugs sampled every 50 cm over an interval of 3 m below the surface, were analyzed for stable isotope analysis (Fig. 17). The $\delta^{18}O$ which varies between −3.85 and −4.52‰, is depleted with respect to the marine Cenomanian signature (*e.g.* Veizer et al., 1999). Some alteration by meteoric water is a likely explanation, but burial recrystallization could also explain such depletion. All samples possess a positive $\delta^{13}C$ signature, which varies between +2.05 and +3.21‰, compatible with Cenomanian marine $\delta^{13}C$ values (*e.g.* Veizer et al., 1999). However, the $\delta^{13}C$ curve displays a consistent continuous decrease of about 1‰ from the base of the profile up to the top Mauddud surface, *i.e.* the Turonian unconformity (Fig. 17). Moreover, the latter surface corresponds to a positive shift of about +0.5‰ in both the $\delta^{13}C$ and $\delta^{18}O$ curves (Fig. 17). Low $\delta^{13}C$ values below a surface are not necessarily evidence of exposure-related modifications (Dickson et al., 2008), but the consistent pattern of both $\delta^{13}C$ and $\delta^{18}O$ along a 3 m thick interval may probably not be explained only by sulfate reduction processes in normal marine conditions. Indeed, the Namak stable isotope

pattern can be best explained by a palaeokarst and/or paleosoil-related alteration, the uppermost and highly altered zone having been eroded during following marine transgression. A similar conclusion can be proposed for the Asaluyeh section. Immenhauser and Rameil (2011) recently warned about a too fast interpretation of such surfaces, but the duration of the hiatus and the isotope profile in Namak support the idea of a critically important surface which is not only a submarine bioturbated starved surface. Indeed, it is also difficult to imagine the development of paleosoils and fluvial micro-conglomerates in Khormuj and Khartang, and not on the axis of the Qatar-Fars high.

6. Discussion

6.1. Sequence stratigraphy

An essential contribution to the stratigraphy of NW Iran presented in this paper is the improved dating of the Mauddud platform, which has been problematic in the past using benthic biozones (Setudehnia, 1978). The earliest Cenomanian age obtained for the transgressive interval overlaying the Mauddud Member, places it in the latest Albian. The combination of the age dating, the change in depositional system from muddy orbitolinid/trocholinid-rich ramp in the Mauddud to the rudist-rich rimmed platforms above, and the well-developed transgressive event, support the correlation with the plate-wide recognized transgression MFS K110 of Sharland et al. (2001). It makes the Mauddud Formation in coastal Fars time equivalent to, for example, the Mauddud Formation in Lurestan (Sharp et al., 2010) and Iraq, and the Natih F and G Members in Oman (van Buchem et al., 2011).

The marls and muddy carbonate ramps of the Albian sequences, represented by the Kazhdumi Formation and Mauddud Member, are present along the entire coastal Fars transect and show modest variations in thickness. Evidence of a positive relief in the Asaluyeh/Namak area during deposition of the Alb-2 sequence is provided by the thickness variation (100–50 m) and the gradual onlap of the Kazhdumi marls on the Dariyan platform (Vincent et al., 2010a,b). First deposits of the Kazhdumi Formation are of early to middle Albian age in Khormuj and Gach, and of late Albian age in Khartang and Asaluyeh (Fig. 18). The thickness of the Alb-3 sequence, including the Mauddud platform, shows little thickness variation along the transect (30–40 m). Within the Mauddud a lateral variation in the sedimentary facies is however observed, indicating a slightly shallower, more confined depositional environment in the Asaluyeh and Namak sections, and deeper water environments along the flanks of the Qatar-Fars high, notably in the marly Gach section (Fig. 18). These observations indicate that the Albian was a time of relative tectonic quiescence in this area.

The tectonically quiet Albian sedimentation is in strong contrast with the Cenomanian/Turonian deposition, when dramatic variations in thickness developed ranging from 350 m in Khormuj to total absence in Namak and Asaluyeh. Recent work in Interior Fars by Piryaei et al. (2010, 2011) reported thickness variations from 150 to 450 m for the same number of Cenomanian and Turonian sequences, and Razin et al. (2010) reported a total thickness of 400 m. This range corresponds to the thickness reported for the Cenomanian/Turonian Natih Formation in Oman, which is approximately 350 m. It thus appears that a thickness in the 300–400 m range is representative for this succession in the southeastern part of the Arabian Plate. Thickness reduction or total absence is attributed to slower relative subsidence or uplift. In the studied area a distinction can be made for the Asaluyeh outcrop, which is situated on the northern tip of the large, N–S oriented anticlinal structure of the Qatar-Fars arch. Since there is no Cambrian salt present over the latter structure, regional tectonic uplift is held responsible for the absence of the Cenomanian and Turonian strata. In the case of Namak the situation is different; here a salt plug is definitely acting, and visible on geological maps and outcrops. Based on the absence of evidence of erosional products, and the good preservation of the Albian Mauddud carbonates, it is assumed that these areas were relative highs and did not receive any sediment during Cenomanian and Turonian times. This does imply that tectonic uplift and probably compression started already in the earliest Cenomanian in the Coastal Fars area.

It is important to note that at the scale of the Arabian Plate, the three Cenomanian sequences, and possibly the Turonian sequence, are correlatable and have a very similar stratigraphic architecture (High Zagros: Razin et al., 2010; interior Fars: Piryaei et al., 2010, 2011; Lurestan: Sharp et al., 2010; Oman: van Buchem et al., 2002). It comprises shallow water carbonate platforms, with a foraminifer and bivalve-dominated interior part, and rudist rudstone and grainstone dominating rims that in downslope (50–100 m) direction grade into intrashelf basinal wackestone and mudstone that are locally organic-rich (van Buchem et al., 2011). What is apparent from all these studies, however, is that the location and extent of the Albian, Cenomanian and Turonian intrashelf basins shifts through time. This has significant implications for the distribution of both reservoir and source rocks. Another characteristic stratigraphic feature are the subaerial exposure surfaces on top of the Cenomanian Ce-3 and the Turonian Tu sequences.

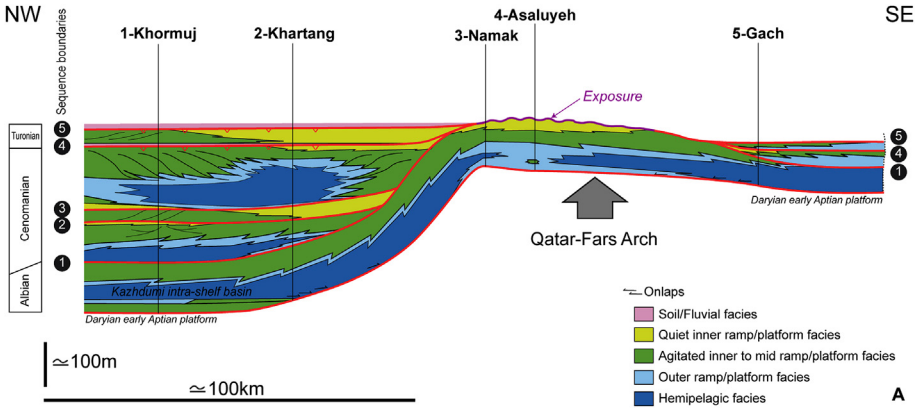

Figure 18. Stratigraphic model based on the correlation of the 5 studied sections, at the SB 5. Noteworthy is the extreme partitioning of sedimentation during the Cenomanian and Turonian along the panel after the end of the Mauddud platform (above SB 1). The multiphase rise of the Qatar-Fars high in the regional geodynamic setting explains this complexity (see the text for further explanation). Note the stacking of all the Cenomanian–Turonian sequence boundaries on the Qatar high.

Bauxite and soil development were observed at these surfaces in several locations in Iran (James and Wynd, 1965; Hajikazemi et al., 2010; Razin et al., 2010; Sharp et al., 2010), but much less in the southern part of the Arabian plate, despite some exposures are reported in the UAE (Champagne, 2012; Deville de Periere et al., 2011), and has been attributed to the impact of the beginning of obduction and the possible development of a foreland bulge (*e.g.* Hollis, 2011).

To summarize, both in the Albian and in the Cenomanian/Turonian, well expressed depositional sequences have been recognized which are attributed to known eustatically-controlled 3rd order sea level variations. From the earliest Cenomanian onwards, this pattern is locally overprinted by strong tectonic activity, acting at both the regional and local scale. A key tectonic factor in this is the distribution of the Cambrian Hormuz salts and the presence of a long term structural high, extending from coastal Fars to the Qatar (Fig. 1), which has been active at different periods throughout the Phanerozoic (van Buchem et al., 2011). Noteworthy is that the endmost Cenomanian to early Turonian period, known as the highest long term sea-level for the Cretaceous (Haq, 2014), corresponds in the study area to the record of some of the most beautiful examples of exposures at the scale of the Arabian plate, which emphasizes the role of tectonics on the sedimentary succession. The termination of the carbonate platforms happened in the Turonian and Coniacian with the onset of ophiolite obduction (*e.g.* Burchette, 1993; Baaske et al., 2006).

6.1.1. Impact of diagenesis on reservoir properties

Near the Cenomanian–Turonian boundary, a widespread exposure is recorded on the northwestern flank of the Qatar-Fars high at the top of the Sequence Ce-3 (surface 4; Fig. 9). It is always difficult to consider outcrops as good diagenetic and petrophysical analogues to subsurface reservoirs. However, in the Khormuj and Khartang sections no extensive cementation was observed below the paleosoils. The underlying limestone is intensively recrystallized, but they also display abundant non-plugged molds and vugs, as well as a patchy “chalky” aspect, demonstrating the alteration of the micrite texture. Moreover, they display limited chemical compaction features (stylolites, solution seams), probably because of an early mineral stabilization during freshwater-related eogenesis, a phenomenon known to efficiently preserve primary porosity in limestone below exposure surface during burial (Wagner and Matthews, 1982; Moore, 2002; Budd et al., 1995; Melim et al., 2002; Heydari, 2003; Dewever et al., 2007). Exposure-related diagenesis may have preserved and/or enhanced reservoir properties in the highstand of the Sequence Ce-3, potentially over a considerable area (Fig. 18). On the southeastern flank of the Qatar-Fars high, no evidences of exposures were observed.

The Sequence Tu displays shallow marine carbonates on the northwestern flank of the high, where it is bounded by two exposure surfaces, whereas the carbonates are significantly deeper on the southeastern flank (Fig. 18). Sediment loading-related subsidence and eustatic variations may explain the shallow marine sedimentation in Khormuj and Khartang, whereas a structural flexure may be invoked to explain the deeper deposits in Gach. The large geographical extension of the exposure associated to the surface 5 on the northwestern flank of the high is explained by a regional uplift of the Qatar-Fars structure. Compressional movements due to ophiolite obduction can easily be invoked to explain this uplift at the end of the Cenomanian since other evidences of this tectonic activity were already reported on the Arabian plate (see discussion above).

The paleogeography at the surface 5, above the Sequence Tu, is similar to that at surface 4, with widespread continental record on the northwestern flank and marine highly condensed deposits on the southeastern flank (Fig. 18). Exposure-related diagenesis was also similar to what has been observed below surface 4 in Khormuj, with a significant preservation and/or enhancement of the reservoir properties of the affected possibly early Turonian limestone (Fig. 18). This positive role of this exposure has also been reported in Upper Sarvak subsurface reservoirs of the Dezful embayment, to the north of the study area (Taghavi et al., 2006).

Noteworthy is that on the axis of the Qatar-Fars high, the potential reservoirs are located in the early Cenomanian Mauddud shallow-marine carbonates (Fig. 18). The depositional facies of the Mauddud platform, dominated by mud-supported orbitolinid-rich textures (Fig. 5), are less favorable than the Sarvak grain-supported rudist-rich facies. However, similarly to what has been observed in the Sarvak below the late Cenomanian and early Turonian exposures, the uppermost Mauddud shallow-marine carbonates in Namak and Asaluyeh sections display a patchy “chalky” alteration, and also limited chemical compaction features. Despite the evidences of exposure at the top Mauddud are not obvious, it nevertheless seems that exposure-related diagenesis altered the limestone and preserved and/or enhanced reservoir properties. Except if fractured, the Mauddud resulting reservoirs would be dominated by microporosity and display high porosity but low to moderate permeability. On the contrary, the Sarvak reservoirs, may be less porous than the Mauddud, would definitely potentially be more permeable due to the occurrence of interconnected macroporosity.

This different behavior of mud-supported versus grain-supported textures affected by meteoric diagenesis in the Cenomanian–Turonian is well illustrated by Hollis (2011), at the scale of the Arabian plate. Deville de Periere et al. (2011) demonstrate the impact of the Top Mishrif Unconformity, which is equivalent to the Top Sarvak surface, on the development of microporous reservoirs in offshore UAE. Closer to the study area in southern Iraq, Mahdi et al. (2013) report the influence of the Mishrif Disconformity (equivalent to surface 4), and the Khasib-Mishrif Unconformity (equivalent to surface 5) on the enhancement/preservation of reservoir properties in the shallow marine carbonates equivalent to the top sequences Ce-3 and Tu.

7. Conclusions

The following conclusions are drawn from this study:

- New dating of the Mauddud Member places it in the latest Albian, and makes it thus time-equivalent, for example, to the Mauddud Formation in Iraq and the Natih F and G Members in Oman;
- Two Albian, three Cenomanian and one Turonian 3rd order sequences have been distinguished in Coastal Fars, which correlate well to time-equivalent sequences reported from other parts of Iran and the Arabian Plate;
- The Albian period is characterized by tectonic quiescence, whereas the Cenomanian/Turonian interval is characterized by dramatic thickness variations (350–0 m) which are attributed to both regional (Qatar High) and local (salt plugs) tectonic uplifts;
- The tectonic activity in the Cenomanian and Turonian, a period of global high relative sea-level, lead to widespread subaerial exposures at the scale of southwest Iran, like in other places of the Arabian plate. Exposure(s) associated with two key sequence boundaries in the end Cenomanian and Turonian (surfaces 4 and 5) display variable expressions at the macroscopic scale in the field (which can be applied to core-scale as well), from thick paleosoil sequences to sharp slightly pitted surfaces, with no direct link with the estimated duration of the

sedimentary hiatus. Thorough petrographic and stable isotope investigation are even necessary to demonstrate the record of exposures in questionable surfaces;

- Long-lasted (more than 1Ma) exposures with thick soil development and/or karst alteration modify significantly the $\delta^{18}O$ of the underlying carbonate through a thick interval, but on the contrary do not modify deeply the $\delta^{13}C$ signature except in the uppermost 2 m below the surfaces. Consequently, the bulk $\delta^{13}C$ of shallow marine carbonate can be used as a constraining tool for sequence stratigraphic correlations. The positive $\delta^{13}C$ excursion associated with the OAE2 characterizes the Turonian 3rd order sequence;
- Although no direct poroperm measurement were performed in this study, a comparison with published data at the scale of the Arabian plate shows that the diagenetic alterations associated with the exposures in the Cenomanian and Turonian may have impacted significantly the reservoir properties below the sequences boundaries, enhancing and/or preserving poroperm in all kind of facies.

Acknowledgments

The results presented in this paper are part of an industry-financed research project that was carried out in close cooperation between the Institut Français du Petrole (IFPEN) and the Exploration Directorate of the National Iranian Oil Company in 2004 and 2005. The following colleagues of the NIOC are acknowledged for their assistance in the acquisition of field data: M. Abbasalinia, M. Alahyari, A. Ashgari, A.R. Ashrafzadeh, Dr. H. Assilian, H. Bahrami Zadeh, A. Faizi, A. Fakoori, B. Fonooni, A. M. Jamali, M. Kavoosi, A. Khosravi Sereshki, M. Maleki, D. Morsalnejad, B. Motamedi, A.-R. Piriaei, Dr. F. Taati, M. Yavari. The management of Exploration, Mr. Mohaddes and Mr. Zadeh-Mohammadi are acknowledged for their support during the project and the permission for publication. The supporting oil companies are acknowledged for discussions of the results. Part of the stable isotope analyses was carried out in the laboratory of Prof. M. Joachimsky (Erlangen University; Germany). Jean Borgomano and one anonymous reviewer are acknowledged for their comments that enhanced the manuscript.

References

Ala, M.A., 1974. Salt diapirism in southern Iran. AAPG Bull. 58, 758–770.
Alavi, M., 1991. Sedimentary and structural characteristics of the paleo-Tethys remnant in NE Iran. Geol. Soc. Am. Bull. 103, 983–992.
Allan, J.R., Matthews, R.K., 1982. Isotope signatures associated with early meteoric diagenesis. Sedimentology 29, 797–817.
Allen, J.R.L., 1986. Pedogenic calcrete in the Old Red sandstone facies (Late Silurian-Early Carboniferous) of the Anglo-Welsh area, southern Britan. In: Wright, V.P. (Ed.), Paleosoils. Their Recognition and Interpretation. University Press, Princeton, pp. 58–86.
Alsharhan, A.S., Narin, A.E.M., 1997. Sedimentary Basins and Petroleum Geology of the Middle East. Elsevier, Amestrdam, p. 843.
Baaske, U.P., Mutti, M., HAIN, M., De Marchi, N., Bertozzi, G., 2006. Control of deep-seated salt tectonics and eustacy on the stratigraphic architecture of Mid-Cretaceous carbonate strata in the central Arabian Gufl, Offshore Iran: a seismic sedimentological study. In: Geo 2006 Middle East Conference and Exhibition, 27–29 Mach, Manama, Bahrain.
Bordenave, M.L., Hegre, J.A., 2005. The influence of tectonics on the entrapment of oil in the Dezful embayment, Zagros foldbelt, Iran. J. Pet. Geol. 28 (4), 339–368.
Burchette, T.P., 1993. Mishrif Formation (Cenomanian-Turonian), Southern Arabian Gulf: carbonate platform growth along a cratonic basin margin. In: Simo, J.A.T., Scott, R.W., Masse, J.P. (Eds.), Cretaceous Carbonate Platforms, AAPG Mem., 56, pp. 185–200.
van Buchem, F.S.P., Simmons, M.D., Droste, H.J., Davies, R.B., 2011. Late Aptian to Turonian stratigraphy of the eastern Arabian Plate – depositional sequences and lithostratigraphic nomenclature. Pet. Geosci. 17, 211–222.
van Buchem, F.S.P., Baghbani, D., Bulot, L.G., Caron, M., Gaumet, F., Hosseini, A., Kayvani, F., Schroeder, R., Swennen, R., Vedrenne, V., Vincent, B., 2010. Barremian – Lower Albian sequence stratigraphy of southwest Iran (Gadvan, Dariyan and Kazhdumi formations) and its comparison with Oman, Qatar and the United Arab Emirates. In: van Buchem, F.S.P., Al-Husseini, M.I., Maurer, F., Droste, H.J. (Eds.), Barremian–Aptian Stratigraphy and Hydrocarbon Habitat of the Eastern Arabian Plate, GeoArabia Special Publication 4, Gulf PetroLink, Bahrain, 2, pp. 503–548.
van Buchem, F.S.P., Razin, P., Homewood, P.W., Philip, J.M., Platel, J.M., Roger, J., Eschard, R., Desaubliaux, G.M.J., Boisseau, T., Leduc, J.-P., Labourdette, R., Cantaloube, S., 1996. High resolution sequence stratigraphy of the Natih Formation (Cenomanian/Turonian) in northern Oman: distribution of source rocks and reservoir facies. GeoArabia 1 (1), 65–91.
van Buchem, F.S.P., Razin, P., Homewood, P., Oterdoom, H., Philip, J., 2002. The Cenomanian Turonian carbonate petroleum system of northern Oman (Natih Formation) – a stratigraphic organization of carbonate ramps and organic-rich intra-shelf basins. Am. Assoc. Pet. Geol. Bull. 86, 21–53.
Budd, D., Saller, A., Harris, P., 1995. Unconformities and Porosity in Carbonate Strata. In: AAPG Memoir, vol. 63. American Association of Petroleum Geologists, Tulsa, p. 313.
Catuneanu, O., 2006. Principles of Sequence Stratigraphy. Elsevier, New York, p. 386.
Chamley, H., 1989. Clay Sedimentology. Springer-Verlag, p. 623.
Champagne, J., 2012. Diagenèse associée aux discontinuités sédimentaires émersives (Formation Natih, Oman). Bordeaux University, p. 449 (unpublished PhD thesis).
Deville De Periere, M., Durlet, C., Vennin, E., Lambert, L., Bourillot, R., Caline, B., Poli, E., 2011. Morphometry of micrite particles in cretaceous microporous limestones of the Middle East: Influence on reservoir properties. Mar. Pet. Geol. 28, 1727–1750.
Dewever, B., Breesch, L., Mezini, A., Swennen, R., 2007. Sedimentological and marine eogenetic control on porosity distribution in Upper Cretaceous carbonate turbidites (central Albania). Sedimentology 54, 243–264.
Dickson, J.A.D., Wood, R.A., Bu Al Rougha, H., Shelb, 2008. Sulphate reduction associated with hardgrounds: lithification afterburn! Sed. Geol. 205, 34–39.
Elrick, M., Molina-Garza, R., Duncan, R., Snow, L., 2008. C-isotope stratigraphy and paleoenvironmental changes across OAE2 (mid-Cretaceous) from shallow-water platform carbonates of southern Mexico. EPSL 277, 295–306.
Erba, E., 2004. Calcareous nanofossils and Mesozoic Oceanic Anoxic Events. Mar. Micropaleontol. 52, 85–106.
Gale, A.S., Kennedy, W.J., Burnett, J.A., Caron, M., Kidd, B.E., 1996. The Late Albian to Early Cenomanian Succession at Mont Risou near Rosans (Dróme, SE France): an Integrated Study (Ammonites, Inoceramids, Planktonic Foraminifera, Nannofossils, Oxygen and Carbon Isotopes). Cretac. Res. 17, 515–606.
Hajikazemi, E., Al-Aasm, I.S., Coniglio, M., 2010. Subaerial expoure and meteoric diagenesis of the Cenomanian-Turonian Upper Sarvak Formation, southwestern Iran. In: Leturmy, P., Robin, C. (Eds.), Tectonic and Stratigraphic Evolution of Zagros and Makran during the Mesozoic-Cenozoic, Geol. Soc. London, Spec. Pub., 330, pp. 252–272.
Haq, B.U., 2014. Cretaceous eustacy revisited. Glob. Planet. Changes 113, 44–58.
Heydari, E., 2003. Meteoric versus burial control on porosity evolution of the Smackover Formation. AAPG Bull. 87, 1779–1797.
Hollis, C., 2011. Diagenetic controls on reservoir properties of carbonate successions within the Albian-Turonian of the Arabian plate. Pet. Geosci. 17, 223–241.
Homewood, P., Guillocheau, F., Eschard, R., Cross, T.A., 1992. Corrélations Haute Résolution et Stratigraphie Génétique: Une Démarche Intégrée. Bull. Cent. Rech. Explor. Prod. Elf-Aquitaine 16, 357–381.
Immenhauser, A., Rameil, N., 2011. Interpretation of ancient epikarst features in carbonate successions – a note of caution. Sed. Geol. 239, 1–9.
Immenhauser, A., Schlager, W., Burns, S.J., et al., 1999. Late Aptian to late Albian sea-level fluctuations constrained by geochemical and biological evidence (Nahr Umr Formation, Oman). J. Sediment. Res. 69, 434–446.
James, G.A., Wynd, J.G., 1965. Stratigraphic nomenclature of Iranian oil consortium, Agreement area. AAPG Bull. 49 (12), 2182–2245.
Jenkyns, H.C., 2010. Geochemistry of Oceanic Anoxic Events. Geochem. Geophys. Geosys. 11, Q03004. http://dx.doi.org/10.1029/2009GC002788.
Joachimsky, M.M., 1994. Subaerial exposure and deposition of shallowing upward sequences: evidence from stable isotopes of Purbeckian peritidal carbonates (basal Cretaceous), Swiss and French Jura mountains. Sedimentology 41, 805–824.
Lewy, Z., Raab, M., 1978. Mid-Cretaceous stratigraphy of the Middle East. Ann. Mus. Hist. Nat. Nice 4, XXXII.1–XXXII.20.
Mahdi, T.A., Aqrawi, A.A.M., Horbury, A.D., Sherwani, G.H., 2013. Sedimentological characterization of the mid-Cretaceous Mishrif reservoir in southern Mesopotamian Basin, Iraq. GeoArabia 18 (1), 139–174.
Matsumoto, T., Nishida, T., Toshimitsu, S., 2003. Early Cenomanian (Cretaceous) ammonoids Utaturiceras and Graysonites from Hokkaido, North Japan. Bull. Geol. Surv. Jpn. 54, 131–159.
Melim, L.A., Wespthal, H., Swart, P.K., Eberli, G.P., Munnecke, A., 2002. Questioning Carbonate Diagenetic Paradigms: Evidence from the Neogene of the Bahamas. IAS 1998 Meeting, p. 27.
Mitchum, R.M., Van Wagoner, J.C., 1991. High-frequency sequences and their stacking patterns: sequence-stratigraphic evidence of high-frequency eustatic cycles. Sediment. Geol. 70, 131–160.
Moore, C.H., 2002. Carbonate Diagenesis and Porosity. In: Developments in Sedimentology, 46Elsevier, Amsterdam, p. 338.
Murris, R.J., 1980. Middle East: stratigraphic evolution and oil habitat. A.A.P.G. Bull. 64, 597–618.

Piryaei, A., Reijmer, J.J.G., Van Buchem, F.S.P., Yazdi-Moghadam, M., Satouni, J., Danelian, T., 2010. The influence of Late Cretaceous tectonic processes on sedimentation patterns along the northeastern Arabian Plate margin (Fars Province, SW Iran). In: Leturmy, P., Robin, C. (Eds.), Tectonic and Stratigraphic Evolution of the Zagros and Makran during the Mesozoic–Cenozoic, Geological Society, London, Special Publications, 330, pp. 211–251.

Piryaei, A., Reijmer, J.J.G., Borgomano, J., van Buchem, F.S.P., 2011. Late Cretaceous tectonic and sedimentary evolution of the Bandar Abbas Area, Fars Region, southern Iran. J. Pet. Geol. 34, 157–180.

Raven, M.J., van Buchem, F.S.P., Larsen, P.-H., Surlyk, F., Steinhart, H., Cross, D., Klem, N., Emang, M., 2010. Late Aptian incised valleys and siliciclastic infill at the top of the Shu'aiba Formation (Block 5, offshore Qatar). In: van Buchem, F.S.P., Al-Husseini, M.I., Maurer, F., Droste, H.J. (Eds.), Barremian–Aptian Stratigraphy and Hydrocarbon Habitat of the Eastern Arabian Plate, GeoArabia Special Publication 4, Gulf PetroLink, Bahrain, 2, pp. 469–502.

Razin, P., Taati, F., van Buchem, F.S.P., 2010. Sequence stratigraphy of Cenomanian–Turonian carbonate platform margins (Sarvak Formation) in the High Zagros, SW Iran: an outcrop reference model for the Arabian Plate. In: van Buchem, F.S.P., Gerdes, K.D., Esteban, M. (Eds.), Mesozoic and Cenozoic Carbonate Systems of the Mediterranean and the Middle East – Stratigraphic and Diagenetic Reference Models, Geological Society, London, Special Publications, 329, pp. 187–218.

Ricou, L.E., 1971. Le croissant ophiolitique peri-Arabe. Une ceinture de nappes mises en place au Crétacé superieur. In: Rev. Géogr. Phys. et Geol. Dyn, XIII, pp. 327–350.

Schroeder, R., van Buchem, F.S.P., Cherchi, A., Baghbani, D., Vincent, B., Immenhauser, A., Granier, B., 2010. Revised orbitolinid biostratigraphic zonation for the Barremian–Aptian of the eastern Arabian Plate and implications for regional stratigraphic correlations. In: van Buchem, F.S.P., Al-Husseini, M.I., Maurer, F., Droste, H.J. (Eds.), Barremian–Aptian Stratigraphy and Hydrocarbon Habitat of the Eastern Arabian Plate, GeoArabia Special Publication 4, Gulf PetroLink, Bahrain, 1, pp. 49–96.

Sehgal, J., Stoops, G., 1972. Pedogenic calcite accumulation in arid and semi-arid regions of the indo-gangetic alluvial plain of erstwhile punjab (India). Their morphology and origin. Geoderma 8 (1), 59–72.

Setudehnia, A., 1978. The Mesozoic sequence in S.W. IRAN and adjacent areas. J. Pet. Geol. 1, 3–42.

Sharland, P.R., Archer, R., Casey, D.M., Davis, R.B., Hall, S.H., Heward, A.P., Horbury, A.D., Simmons, M.D., 2001. Arabian Plate Sequence Stratigraphy. In: GeoArabia Special 2. Gulf Petro Link, Bahrain, p. 371.

Sharp, I., Gillespie, P., Morsalnezhad, D., Taberner, C., Karpuz, R., Verges, J., horbury, A., Pickard, N., Garland, J., Hunt, D., 2010. Stratigraphic architecture and fracture-controlled dolomitization of the Cretaceous Khami and Bangestan groups: an outcrop case study, Zagros Mountains, Iran. In: van Buchem, F.S.P., Gerdes, K.D., Esteban, M. (Eds.), Mesozoic and Cenozoic Carbonate Systems of the Mediterranean and the Middle East – Stratigraphic and Diagenetic Reference Models, Geological Society, London, Special Publications, 329, pp. 343–396.

Stonely, R., 1981. The geology of Kuh-e- Dalneshin area of southern Iran and its bearing on the evolution of southern Tethys. J. Geol. Soc. Lond. 138, 509–526.

Strasser, A., Pittet, B., Hillgartner, H., Pasquier, J.-B., 1999. Depositional sequences in shallow carbonate-dominated sedimentary systems: concepts and definitions. Sediment. Geol. 128, 201–221.

Taghavi, A.A., Mork, A., Emadi, M.A., 2006. Sequence stratigraphically controlled diagenesis governs reservoir quality in the carbonates Dehluran field, southwest Iran. Pet. Geosci. 12, 115–126.

Vahrenkamp, V., 2013. Carbon-isotope signatures of Albian to Cenomanian (Cretaceous) shelf carbonates of the Natih Formation, Sultanate of Oman. GeoArabia 18 (3), 65–82.

Vail, P.R., Audemard, F., Bowman, S.A., Eisnet, P.N., Perez-Cruz, C., 1991. Signatures of tectonics, eustasy and sedimentology – an overview-. In: Einsele, G., Ricken, W., Seilacher, A. (Eds.), Cycles and Events in Stratigraphy. Springer, Berlin/Heidelberg/New York, pp. 617–659.

Veizer, J., Ala, D., Azmy, K., Bruckschen, P., Buhl, D., Bruhn, F., Carden, G.A.F., Diener, A., Ebneth, S., Godderos, Y., Jasper, T., Korte, C., Pawelleck, F., Podhala, O.G., Strauss, H., 1999. $^{87}Sr/^{86}Sr$, $\delta^{13}C$ and $\delta^{18}O$ evolution of phanerozoic seawater. Chem. Geol. 16, 59–88.

Vincent, B., van Buchem, F.S.P., Bulot, L.G., Immenhauser, A., Caron, M., Baghbani, D., Huc, A.Y., 2010a. Carbon-isotope stratigraphy, biostratigraphy and organic matter distribution in the Aptian – Lower Albian successions of southwest Iran (Dariyan and Kazhdumi Formations). In: van Buchem, F.S.P., Al-Husseini, M.I., Maurer, F., Droste, H.J. (Eds.), Barremian–Aptian Stratigraphy and Hydrocarbon Habitat of the Eastern Arabian Plate, GeoArabia Special Publication 4, Gulf PetroLink, Bahrain, 2, pp. 139–197.

Vincent, B., Swennen, R., Jalali, M., Baghbani, D., van Buchem, F.S.P., 2010b. Regional unconformities in the Cenomanian and Turonian limestone of southwest Iran (Sarvak Formation): sub-aerial exposures, diagenetic patterns and impact on reservoir properties. In: EAGE 2nd Arabian Plate Workshop, Abu-Dhabi January 2010.

Wagner, P.D., Matthews, R.K., 1982. Porosity preservation in the Upper Smackover (Jurassic) carbonate grainstone, walker creek field, Arkansas – response of paleophreatic lenses to burial processes. J. Sediment. Petrol. 52, 03–18.

Wennberg, O.P., Azizzadeh, M., Aqrawi, A.A.M., Blanc, E., Brockbank, P., Lyslo, K.B., Pickard, N.P., Salem, L.D., Svana, T., 2007. The Khaviz anticline: an outcrop analogie to giant fractured Asmari Formation reservoirs in SW Iran. In: Lonergan, L., Jolly, R.J.H., Rawnsley, K., Sanderson, D.J. (Eds.), Fractured Reservoirs, Geol. Soc. London, Spec. Pub. 270, pp. 23–42.

Wiedmann, J., Schneider, L., 1979. Cephalopoden und Alter der Cenoman-Transgression von Mülheim-Broich, SW-Westfalen. In: Wiedmann, J. (Ed.), Aspekte der Kreide Europas, IUGS ser. A, 6, pp. 645–680.

Wiedmann, J., Kaplan, U., Lehmann, J., Marcinowski, R., 1989. Biostratigraphy of the Cenomanian of NW Germany. In: Cretaceous of the Western Tethys, Proceedings of the 3rd International Cretaceous Symposium, Tübingen 1987, pp. 931–948.

Wright, C.W., Kennedy, W.J., 1987. The Ammonoidea of the Lower Chalk. Part 2. Palaeontogr. Soc. Monogr. 573, 127–218.

Wright, C.W., Kennedy, W.J., 1996. The Ammonoidea of the Lower Chalk, Part 5. Palaeontogr. Soc. Monogr. 320–403.

Wynd, J.G., 1965. Biofacies of the Iranian Consortium – Agreement Area, Report 1082. N.I.O.C. Report, Unpublished.